LAPP-EXP-92.03
NOVEMBER 1992

A HIGH RESOLUTION JET ANALYSIS FOR LEP

HARIRI Saadeddine*
Laboratoire d'Annecy-Le-Vieux de Physique des particules
Chemin de Bellevue - F74941 ANNECY LE VIEUX CEDEX, FRANCE

ABSTRACT

In this paper, we report about a high resolution multijet analysis of hadronic events produced in e^+e^- annihilation at a C.M.S. energy of 91.2 GeV. The quality of the analysis is based on the following : 1) The rate of hard 3-jet events is about 2 to 3 times higher than the one quoted using event shape variables and cluster analysis [1] ; 2) The analysis is linear in particles' momenta and consequently it is perfectly compatible with hadron calorimetry techniques ; 3) It requires a good resolution on the jet axis only. This is easily achieved in any medium quality experiment. High resolution on the jet energy is not required ; 4) It has a minimal sensitivity to the theoretical uncertainties concerning the 3-jet rate and measured 3-jet variables. Three and four jet events are separated and the 3-jet phase space is clearly defined ; 5) The analysis establishes a clear separation of perturbative effects that govern the 3-jet rate and kinematics from the non-perturbative effects related to the jet hadronization process ; 6) The jet hadronization variables (P_T and rapidity) are calculated for each jet using the jet axis and NOT the event axis (thrust or sphericity). Global variables characterizing the event as a whole are also calculated ; 7) Comparing this analysis to the commonly used event shape variables and clusters, we find that these analyses lead to a large theoretical uncertainty and large systematical error concerning the 3-jet rate and dynamics.

---

* Fellow of the French Ministry of Foreign Affairs ; Id076500G 1 2201E permanent address : Lebanese Univ., Faculty of Sc. SECTION-1
CENTRAL ADMINISTRATION, MATHAF, BEIRUT, LEBANON.

Hadronic events produced in e^+e^- annihilations are generated using the Monte carlo program JETSET7.3 with its two options : Matrix Element (M.E.) and Parton Showers (P.S.). Detailed description of the program can be found in the reference manual distributed by the author [2]. The shower option is used with its default parameter values while the M.E. option is used with an invariant mass cut $Y_{CUT} = 0.01$ instead of 0.02. This choice ensures a better continuity in the evolution of the event shape variables.

I) THE JET BUILDING ALGORITHM.

To achieve a full reconstruction of unbiased jets of hadrons, we proceed as follows :

a) Clusters : clusters are defined as groups of particles going almost in the same direction. To initialize the program, the particles of the event are ordered according to their energies : $E_i > E_{i+1}$. Starting with the fastest ones, any pair of particles with a relative angle $\theta_{ij} \leq 2\,\delta$ is replaced by a single particle having as energy the sum of the energies and as direction the vector obtained by adding the 3-momenta. An axis defining the direction of each cluster is obtained. Repeating the procedure and using as initial axes the axes of the clusters, the energy and direction of each cluster are redefined. This last step is repeated twice in order to get a precise determination of the cluster axis. We used $\delta = 15°$.

b) Prejets : The axes of the clusters are now used as input. Each particle is associated with the closest to it axis and the prejet energy and axis are then redefined. If the prejet energy is less than E_{min} the prejet axis is discarded and the prejet particles are redistributed among the remaining prejets. Whenever a prejet is removed the axes and energies of the surviving ones are updated. Repeating the procedure twice, we end up with prejets having an arbitrary angular width and a minimal energy equal to E_{min}. We used $E_{min} = 3$ GeV. The rate of prejets then obtained is shown on Fig. 1.

c) Jets : Using as input the above prejets, we require that the invariant mass, Y_{ij} (= $(E_i/E_{beam}) * (E_j/E_{beam}) * (1-\cos\theta_{ij})$, E_{beam} = beam energy = half of the visible energy E_{vis}) to be above a minimum value Y_{min}. When a pair of prejets fails this requirement, the lower energy prejet is removed and its particles are redistributed. Each time a prejet is removed the axes and energies of the jets are recalculated. We end up with a set of jets having a minimal energy larger than 3 GeV and a minimal angle between the axes of neighbouring jets above 30°. The minimal invariant mass of any pair of jets is equal to Y_{min}. For $Y_{min} = 0.04$ the jet rate distribution is shown on Fig.2.

II) THE 3-JET KINEMATICS AND VARIABLES.

a) Variables : The 3-jet kinematics is described in terms of the jet scaled energy :

$$X_i : E^i_{jet}/E_{beam} = 2. * E^i_{jet}/E_{vis}$$

$$X_1+X_2+X_3 = 2 \qquad (1)$$

The angles θ_i are defined as :

θ_i = angle between jets (j,k) ;
(i,j,k) = 1,2,3)
$\theta_1 + \theta_2 + \theta_3 = 360°$

Consequently the following relation holds :

$$X_1/\sin\theta_1 = X_2/\sin\theta_2 = X_3/\sin\theta_3 \qquad (2)$$

The invariant masses Mi are :

$$M_i = X_j * X_k * (1. - \cos\theta_i) \qquad (3)$$

This implies that : $M_i = 2.(1. - X_i)$. Our invariant mass cut Y_{min} is equivalent to the thrust cut : $X_1 \leq 0.98$. Notice that the mass M_i is twice the invariant mass m_{ij} expressed in unit of E_{vis} : $M_{ij} = 2.(E_{ij}/E_{vis}) * (E_j/E_{vis})(1. - \cos\theta_i) = 0.5\, M_K$. The Y_{cut} variable is expressed in terms of E_{vis} and consequently $Y_{cut} = 0.01$ coresponds to $Y_{min} = 0.02$.

The jet energy in a 3-jet event is computed from angles according to equations (1,2). The invariant mass M_1 of a 3-jet CANDIDATE is obtained from equation 3. The event selection corresponds to $M_1 \geq 0.04$ ($X_1 \leq .98$). This is a highly important point in minimizing the experimental systematical error associated with jet selection criteria. Indeed a good detector would give a good angular resolution on the jet direction and a good resolution on the overall energy of the event. There is no such detector that ensures local energy and momentum conservation for each jet separately. Our Monte carlo program does, at the fragmentation level, keep track of the jet direction and globally conserves energy and momentum (global constraints only !). The distribution of (E_1/X_1) where E_1 is the scaled measured energy of jet 1 is shown on Fig.3. The curve represents the results of an ideal experiment. In reality, the experimental resolution on the jet energy is much worse. A calorimeter detector would give a high resolution on (X_i,θ_i) regardless of the missing low energy particles. The PETRA experiments (MARKJ calorimeter, TASSO charged track detector) achieved already good results in this respects. Presently used detectors at LEP, are expected to have a much higher performance.

In this analysis, our cut on the prejet energy $E_{min} = 3$ GeV, coresponds to $E_3 \geq 0.66$. The Y_{min} cut as implemented in the jet reconstruction phase implies : $X_1 < .98$; $X_3 \geq 0.1$; $\theta_1 > 35°$; $\theta_3 \leq 175°$. Experimental error (< 30 %) on the energy of the third jet does not lead to the 3-jet event destruction or misidentification.

On Fig. (4,5), we show the distribution of X_1 and of θ_3 for our 3-jets of hadrons. Needless to mention that our problem has only 2 free parameters : $(X_1 \rightarrow \theta_1)$; $(X_3 \rightarrow \theta_3)$. As to the importance of the Y_{min} cut in setting the boundaries of the 3-jet phase space, the distributions of the variable X_1 for partons' and hadrons' 3-jet events are shown on Fig.6.

b) Jet intrinsic width :

In a jet analysis, the jet angular width intervenes at many levels. Although this point is not specific to the 3-jet kinematics, we prefer to discuss it here for clarity reasons and compactness of the article. To this end, an energy flow parameter is defined as follows :

$$x(\theta) = E(\theta)/E_{jet}$$

where $E_{(\theta)}$ is the sum of the energies of all particles that are emitted with respect to the jet axis at an angle smaller or equal to θ. Energy flow diagrams for two and three jets of hadrons are shown on Fig.7. We find that x (15°) > 80 % for all jets. Consequently our program is correctly initialized since an original cluster contains about 80 % of the jet energy. This ensures a quick and successful convergence of the jet reconstruction procedure. As to the jet angular width, the diagrams show that no upper limit on the jet angular spread is preset in the program.

A deeper problem, consists of studying the jet angular width at the parton level. Parton showers do have their own intrinsic width at the generation level before fragmentation. The partons of the shower have a P_T spectrum and rapidity spectrum with respect to the shower axis. Consequently, the showering mechanism produces an initial P_T that will add to the hadronization P_T when partons are fragmented. In the M.E. approach, this initial width of the jet does not exist. Nevertheless, since we impose the $Y_{min} = 0.04$ cut on jets generated with $Y_{cut} = 0.01$, events generated with 3 energetic partons are sometimes classified as two jets. In the two jet sample, one of the jets will contain two neighbouring high energy partons. Fig. 8 shows the energy flow diagram for two jets of partons and Fig.9 produces the same distribution for the 3-jet case. We notice that hadronized and unhadronized parton showers have comparable width. It follows that the transverse momentum, with respect to the jet axis, of the particles produced by shower hadronization is fixed in principle by the initial width of the shower The additionnal P_T brought in by the fragmentation function is not more than a second order correction. Table 1 establishes the correspondence between the average P_T used to fragment the jets (σ) and the effective P_T measured after hadronization. The effective measured sigma $\sigma_{eff} = \langle P^2_T \rangle$ is also produced. We notice that a $\sigma_{eff} = 380$ MeV is obtained for σ(P.S.) = 30 MeV and σ (M.E.) = 300 MeV. For the same σ_{eff}, the two sets of events will have different P_T spectra because the tail of the P_T-distribution in the P.S. option is not controlled by σ but by the shower width (α_s ?). In the M.E. option, the initial width 4°-5° of the jet of partons (Fig.8) due to the Y_{min} cut is the only source of intrinsic P_T. The impact of the jet initial width on rapidity spectra, will be discussed later.

We conclude, here, that if the two jet momentum structure is to be fairly studied then the two jet events should be selected using a low Y_{min} cut (Y_{min} : 0.02 ?). In this case, the M.E. two jet will have no initial width and the P.S. two jet will carry the shower width.

Figures (10,11) show the rapidity distributions for two and three jet events of the M.E. Monte carlo. For each particle two rapidities are computed : one with respect to the jet

axis Y_A and the other with respect to the thrust axis Y_T. Spectra of the rapidity Y_A show the expected bump at Y = 3 (θ.=.5°). Discarding this anomaly due to analysis*, these distributions do correspond to a real plateau. At the same time, the Y_T distribution calculated for these events have a strongly curved shape. Similar plots for the P.S. Monte carlo are shown on Fig. (12,13). Here the Y_A bump at $Y_A = 3$ is smoother and wider since two neighbouring partons in the M.E. option correspond to two neighbouring showers in the P.S. option. In both cases, a flat Y_A spectrum is seen while the Y_T spectrum keeps its unusual form. Combining the two and three jet samples and recalculating the (Y_A,Y_T) distributions we obtain the curves of fig. (14,15).

First, we notice that Y_A distributions for 3-jet events present a dip at $Y_A = 0$. Indeed, if a particle is in the event plane and its momentum is perpendicular to the jet axis ($Y_A = 0$) then this particle is associated with one of the neighbouring jets (since it becomes closer to one of them). Similar situation does not occur for two jet events and no dip is seen there. Second, combining two Y_A distributions having different plateau width can only bring confusion. We do it in order to compare the combined Y_A distribution with the Y_T one. In fact, published data is presented in terms of the Y_T combined spectrum (Ref.1.a, Fig.15a and 16a). Comparing Fig.14 to Fig.11 we see that the Y_A - plot still carry some information while the Y_T one becomes too complicated. Two Y_T distributions with no plateau at all, produce after combination a weak plateau due to the fact that they have different widths and displaced peaks. Consequently, a Y_T distribution computed for all events does not carry any useful information. Its fake plateau is quite misleading. It proves nothing that may concern the momentum structure of the observed jets. Forcing a Monte Carlo to produce a clear Y_T plateau may dangerously destroy the physics incorporated in the program.

From this paragraph, we conclude that our Y_A-distributions separately calculated for two jet and three jet samples do really represent what we expect from fully reconstructed unbiased jets. Other topological variables (P_T,P_{Tin},T) will be presented in a separate section.

We close this paragraph by a short comment about the P.S. Monte carlo. In this program a cutoff parameter M_{min} (PARJ(82)) determines the minimal energy of a parton that can radiate. Since we do not know at which energy real quarks and gluons stop radiating, we tried to estimate the sensitivity of our results to the value of this parameter. Needless to mention that M_{min} controls the shower width, P_t spectra and also the jet rate. Plotting the rate of reconstructed 3-jets as a function of M_{min}, we obtain (for the same value of lambda QCD) the curve shown on Fig.16. The rate of 3-jets is maximum for M_{min} = 3 to 7 GeV. It drops by 10 % when this parameter goes from 3 GeV to 1 GeV (default value). We leave this theoretical point as an open question that concerns theoreticians. Here, in

* In a later paper the detailed properties of the jet fragmentation function will be studied. The twojet definition used here is an introduction to the more precise one that we will use in a coming paper.

this paper, all distributions and numbers are calculated using the program original settings.

c) The 3-jet phase space :

When selecting 3-jet events, it is highly important to define the boundaries of a kinematical region (phase space volume with no holes inside) where 3-jet events are produced. In our case, this is done by the Y_{min} cut. In fact, we could use the (δ,ε) parameters of the analysis proposed by Ellis [3 ; Sjostrand article]. They correspond to the (E_{min},δ) variables introduced to define prejets. The M.E. Monte Carlo uses an invariant mass cut to define the 3-jet phase space. A bigger trouble would occur if the chosen 3-jet phase space allows the production of a mixture of hard 3-jets, soft 3-jets and fake 3-jets generated by a wide hadronization of two partons final states. Such a situation was, to certain extent, unavoidable at PETRA energies. But now at the LEP energies where getting evidence for 3-jet production is of no use at all, precision measurement is a must. Most of the presently used analyses (Thrust, sphericity, oblateness, jet mas.) were developed at PETRA with a main purpose defined by detecting deviations from simple two jet picture.

In our analysis, only hard 3-jets are accepted. Using the M.E. Monte Carlo where only hard partons are produced, we have calculated the distribution of the number of partons in our two and three jet samples. The distribution is shown on Fig.17 where the events with five partons correspond to 4 partons with a hard photon due to Q.E.D. radiative correction. We notice the absence of two parton final states in our 3-jet sample. The insensitivity of our 3-jet rate to the used hadronization model is shown on Fig.18 where the rate of 3-jet events is calculated for different values of the hadronization P_t. The covered wide P_t-range is quite sufficient to show that we have really discoupled fragmentation effects from Q.C.D. effects.

We conclude that we have defined fixed and continuous kinematical region where 3-jets of hadrons and/or partons are equally treated. The X_1-spectrum of Fig.6 is the same for partons' and hadrons' 3-jet events. A similar high resolution spectrum is, obtained for the angle θ_3.

A deeper test of QCD matrix element is achieved using the double differential jet cross section. In a first order calculation, the cross section reads :

$$D\sigma/DX_1\,DX_2 = \sigma_0 * (\alpha_s/2\pi) * (X^2_1 + X^2_2)/(1. - X_1)(1. - X_2) * C_F$$

were σ_0 is the lowest order cross section and C_F is the colour factor. Setting $FX_1X_2 = (X^2_1+X^2_2)/(1-X_1)(1-X_2)$ and calculating the average $\langle FX_1X_2\rangle$ per bin of X_1 (here we take $dX_1 = 0.02$) we construct the function :

$$G(X_1) = 1/N * DN/DX_1 * 1/\langle FX_1X_2\rangle$$

The distribution of $G(X_1)$ should be a flat one in a first order QCD model. For $O(\alpha^2_s)$ models the $G(X_1)$ plot is curved. Using an arbitrary normalization factor, the plot of

$G(X_1)$ is calculated using about 100 thousands of 3-jet events. The result is shown on Fig.19.

Another aspect showing the performance of our multijet approach is the representativity of the selected 3-jet sample. Our 3-jet rate is 40-50 % while in the famous JADE resolution algorithm this rate remains below 20 % (Ref.1.a ; R_3-plot). This large difference in the event rate is accompanied by a large difference in precision as shown on Fig.3 and as it will be explained here below.

III. TOPOLOGICAL APPROACHES.

a) Light jet mass :

In a 3-jet event, the first jet is the light jet while jets 2 and 3 together form the heavy jet. Using the 3-jet variables, the light jet mass is :

$$M^2_l = (E^2_j - P^2_j)l = X^2_1 - (T_1 X_1)^2 = X^2_1(1. - T^2_1)$$

where T_1 is the thrust of the first jet :

$$\rightarrow X_1)_l = M_l/(1 - T^2_1)^{1/2}$$

Comparison of the value of X_1 obtained from the light jet mass to the value of X_1 that we calculate reduces simply to a comparison of X_1 to the observed energy E_1 of the first jet measured in units of Ebeam. Fig.3 has shown already the error due to approximating the 3-jet thrust X_1 by the scaled observed energy of Jet 1.

b) Heavy jet mass :

The heavy jet mass is the invariant mass of the jets 2 and 3 when correctly reconstructed. Using our variables, we get :

$$M^2_h = (X_2 + X_3)^2 - (T_1 * X_1)^2 = (2 - X_1)^2 - (T_1 * X_1)^2$$

$$M^2_h = M^2_l + 4(1 - X_1) \text{ OR } X_1(M_h, M_l) = 1. - 0.25(M^2_h - M^2_l)$$

Evaluating this value of X_1 using the measured mometa and energies of the jets and plotting the ratio $X_1(M_h, M_l)/X_1$ where X_1 is the thrust of our 3-jet, we obtain the distribution shown on Fig.20. We conclude that the functions $X_1(M_h, M_l)$ and $X_1(M_l, T_1)$ are basically the same with the same hadronization component. One could also express X_1 in terms of the thrusts (T_l, T_h) of the light and heavy jets respectively. We conclude that (M_l, M_h, T_l, T_h) carry approximately the same mixture of perturbative and non-perturbative components. To that mixture one should add the experimental resolution on energy and direction of individual particles (one normally assumes a perfect detector simulation).

c) Oblateness :

Supposing that we obtain a reasonable expression of X_1 in terms of the commonly used hadronic variables (as above), the 3-jet variables $(X_2, X_3, \theta_{1,2,3})$ could be computed if one of them or a function of them is expressed in terms of the hadronic parameters. In the

oblateness analysis the variable Major computed using the particles of the heavy jet and measured in units of E_{beam}, reads :

$$M_b = X_T \equiv X_2 * \sin\theta_3 + X_3 * \sin\theta_2 = 2. * X_2 * \sin\theta_3$$

For given values of (X_1,X_T), the variables $(X_2,X_3,\theta_{1,2,3})$ can be easily constructed graphically. Computing M_b using the particles of the second and third jet as they are fully reconstructed in our analysis, we compare the distributions of M_b and X_T (Fig.21).

We first notice that our X_T is systematically higher. This is explained in terms of the jet energies as follows :

$$M_b = (E_2*T_2) * \sin\theta_3 + (E_3*T_3) * \sin\theta_2$$

assuming perfectly defined angles, the source of error in this direct evaluation of M_b would come from the systematical errors on (E_2,E_3,T_2,T_3). Even if (E_2,E_3) are ideally measured, the hadronization component of M_b generated by (T_2,T_3) will make M_b strongly dependent on P_T. The distribution of (θ_2,θ_3) obtained using $(X_1(M_h,M_l),M_b)$ are quite far from the ones we obtain. Failing in reconstructing the 3-jet variables using hadronic parameters, we conclude that a jet approach leads easily to jet variables and to well defined hadronization variables (y,P_T,T,etc). Going in the opposite direction leads nowhere. Event shape variable are based on a two jet picture with two hemispheres defined by the thrust axis or sphericity axis. An extrapolation of this analysis to 3-jet and 4-jet region does not look to be a safe or wise choice.

d) <u>The hadronic thrust T</u> :

This variable is often confused with X_1 although the difference is quite big. For 3-jet events, the thrust T reads :

$$T = [T_1 * X_1 - (T_2 * X_2 * \cos\theta_3 + T_3 * X_3 * \cos\theta)]/2$$

For a perfectly balanced event, this reduce to :

$$T = 2T_1 * X_1/2 = T_1 * X_1$$

or $$X_1(T_1,T) = T/T_1$$

This final expression of T, shows the complexity of the variable T. The purely perturbative variable X_1 is weighted by the jet hadronization parameter T_1. The distribution of T for 3-jet events is shown on Fig.22 for the two sets of events used.

<u>IV. JET FRAGMENTATION PROPERTIES.</u>

In a previous paragraph, we have stressed the fact that our two Monte carlo models do have the same average P^2_T with respect to the jet axis. We have also, fairly presented the rapidity distributions by normalizing the probabilities to unity in order to cancel out any difference in multiplicity. Our analysis was able to resolve the difference in momentum structure between the two copnsidered types of jets in terms of the true rapidity Y_A. Here, in this paragraph, we present P_T-spectra.

Fig.23 shows the distribution of P^2_T relative to the jet axis for the particles of Jet1 in our 3-jet sample. The difference in the high P_T region between the two models is clearly

resolved by our program. As a consistency chek, we plot the P^2_T spectrum for Jet1 and for the two jet sample. Fig.24 shows that the two spectra do really coincide.

Computing P_T spectra with respect to the event axis, a large difference is found between 2 and 3 jet events. Indeed, the particles of the second and third jets in a 3-jet event will have a very high P_T with respect to the event axis. The distributions are shown on Fig.25. Going from Fig.24 to Fig.25, a great difference is seen although the hadronization process is the same. The artificial difference is generated by the angles θ_2 and θ_3 of the 3-jet. If the 2 and 3-jet samples are combined and the particles P_T is measured with respect to the event axis there would be no way to tell what is perturbative and what is non-perturbative in the obtained spectrum. This is the same conclusion that we learned from the Y_T combined spectrum. A topological approach to 3-jet physics can never disentangle perturbative and non-perturbative effects in anyone of the commonly published spectra ($Y,P_T,T,.$). This is the weakest point of global approaches.

From the distribution of (X_1,θ_3), we have learned that P.S. and M.E. models differ in the kinematics of their 3-jets. From Fig.23 we learned that they do also differ in P_T-spectra. If the two effects are to be combined then a P^2_{Tin} would do the job. On Fig.26, we see that M.E. 3-jets have a wider P_{Tin} distribution although their average X_1 is higher and their P_T spectrum cuts off faster. It would be difficult to explain the P^2_{Tin} distribution if we do not know in advance that M.E. jets have lower multiplicity, higher average momentum per particle and smaller width. With this information the apparent contradiction betwwen P^2_T spectrum with respect to the jet axis and P^2_{Tin} spectrum is easily resolved !. Once more, we feel the complexity of topological variables where different processes contribute concurrently to the distribution of each of them. At the same time the precision, clarity and simplicity emerge as the main features of our multijet analysis.

ACKNOWLEDGEMENTS.

I would like to thank the Director of the LAPP for the kind hospitality extended to me at his laboratory. My thanks go also to the French Ministry of Foreign Affairs that offered me this two months fellowship at Annecy and to the Dean of the faculty of Sciences of the Lebanese University.

I would like to thank the Annecy Computer Group and especially Mrs Denise Dufournaud for their kind help and technical assistance.

Finally, I would like to thank Mrs Christiane Le Marec who typed not only this report but also my previous theses and reports with a lot of care and extreme sympathy.

REFERENCES

1) a) Properties of hadronic Z decays and test of QCD generators,
ALEPH Collab., CERN-PPE:92-62 (1992)
b) Determination of α_s from hadronic event shapes measured on the Z resonance
L3 Collab., P.L. B284 (1992), P.P. 471-481
c) ALEPH Collab., D.Decamp et al., Z. Phys. C49 (1991) 623
d) DELPHI Collab., P.Abreu et al.,
Determination of α_s in second order QCD in hadronic Z decays,
CERN-PPE/91-181 (revised)
e) OPAL Collab., P.D. Acton et al.,
A global determination of α_s (MZ) at LEP, CERN-PPE/92-18
f) L3 Collab., B.Adeva et al., P.L.B257 (1991) 469
g) OPAL Collab., P.D.Acton et al., P.L.B276 (1992) 547
h) ALEPH Collab., D.Decamp et al., P.L. B257 (1991) 479
i) ALEPH Collab., Contribution to the 26th International Conf. on High Energy Physics, Dallas, Texas, Aug.6-12, 1992

2) A manual to the Lund Monte Carlo for jet fragmentation and e^+e^- physics.
Contact T.Sjostrand, CERNVM TORSJO

3) a) Z Physics at LEP, Vol.3, P.P. 143-340, CERN89-08
b) R.K.Ellis, D.A.Ross, A.E.Terrano
Nucl. Phys. B178 (1981) 421.

TABLE-1

P.S.

SIGMA MeV	< PT2 > GeV2	ROOT(< PT2 >) MeV
30	0.145	380.8
150	0.16	400.
300	0.2	447.2

M.E.

200	0.1217	348.85
300	0.148	384.7
400	0.184	428.95

THETA	5.	10.	15.	20.	25.	30.
Y	3.13	2.44	2.03	1.74	1.51	1.32

Figures Captions

The sum of the probabilities quoted on the Y-axis of the distributions is 100 for all curves. No division by the binwidth is done. The binwidth is visible on the plots themselves. Smoothed curves are a pure eye fit to the calculated points represented on each plot by an open circle or triangle.

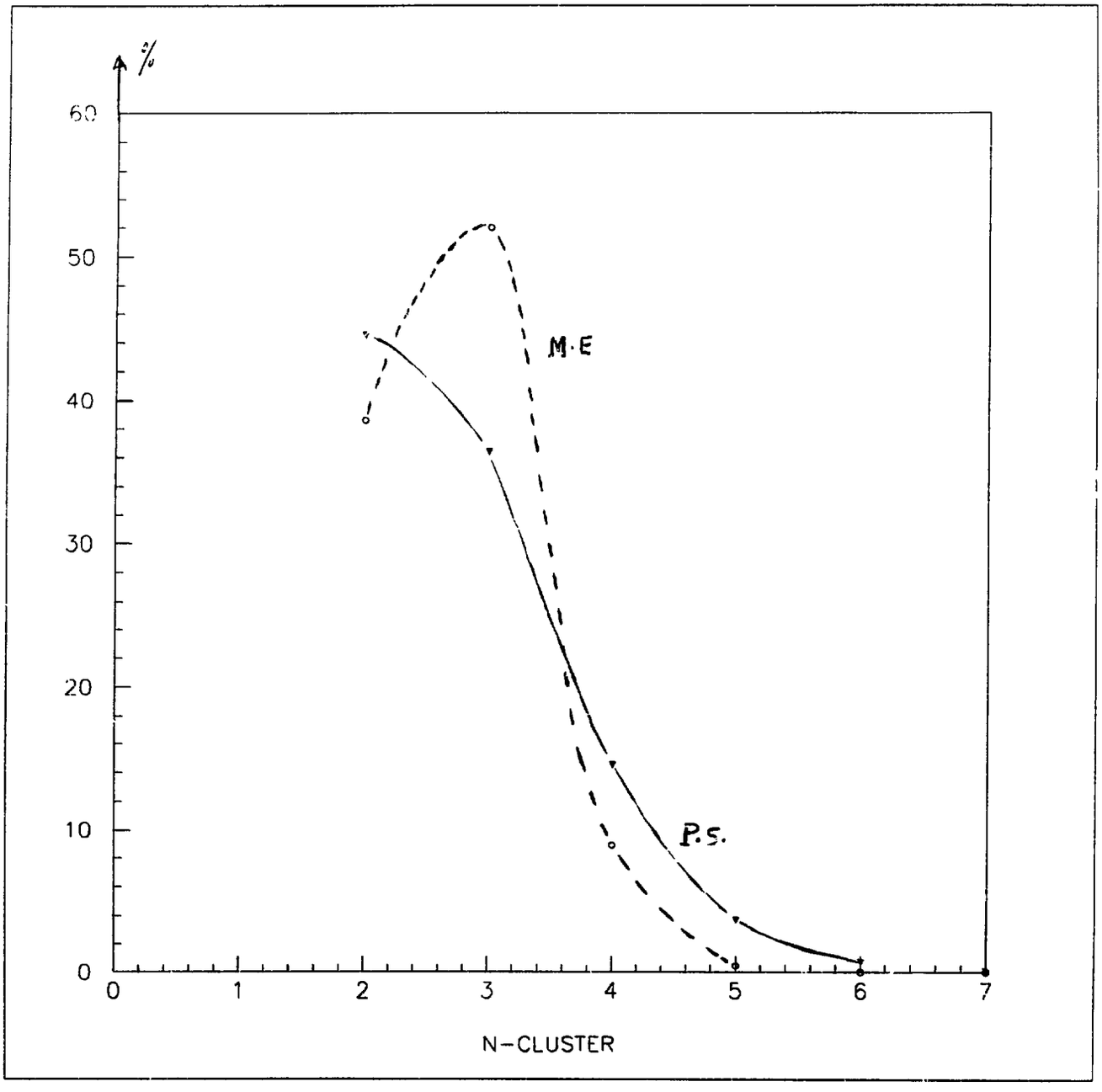

Fig.1

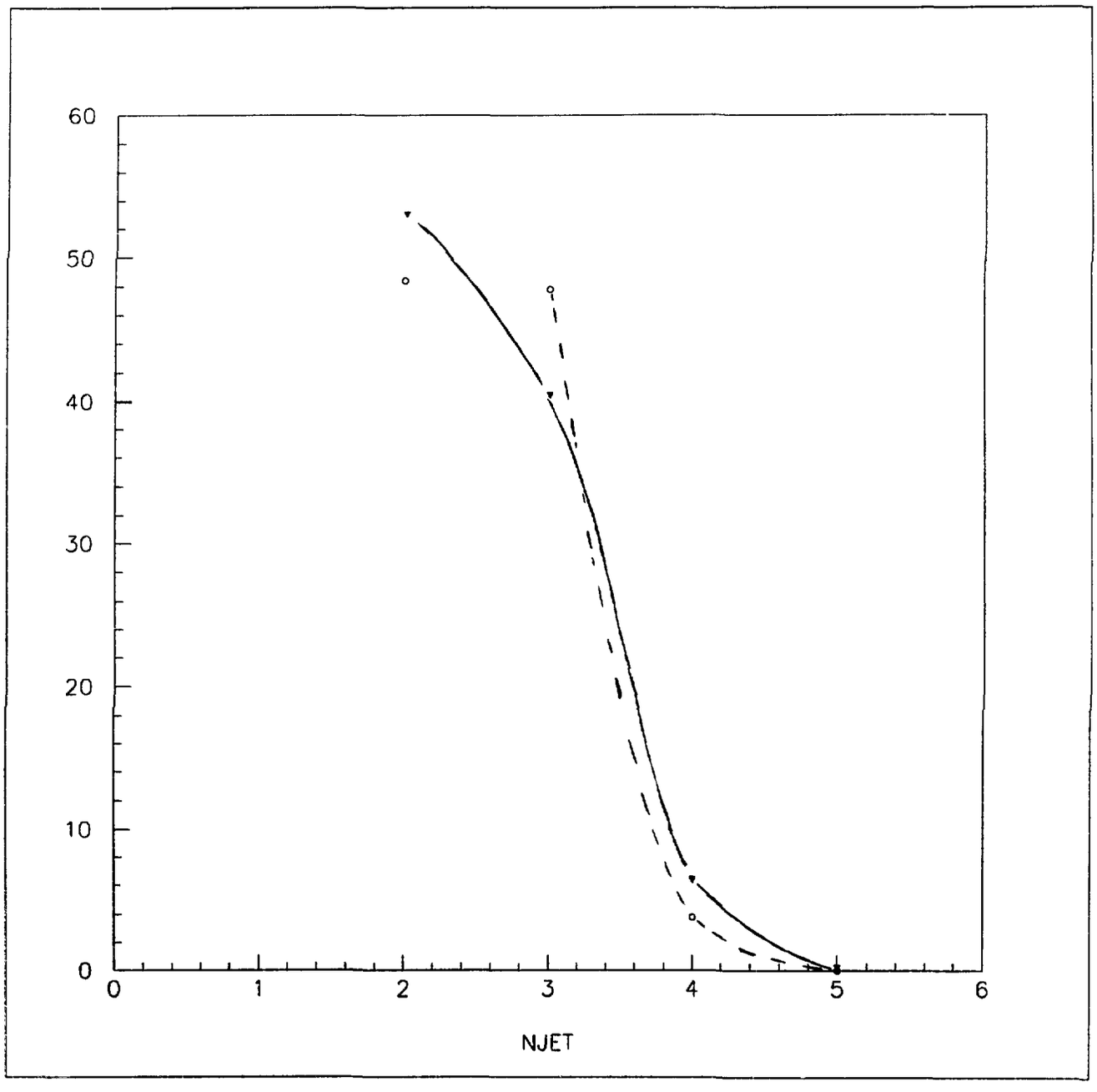

Fig.2

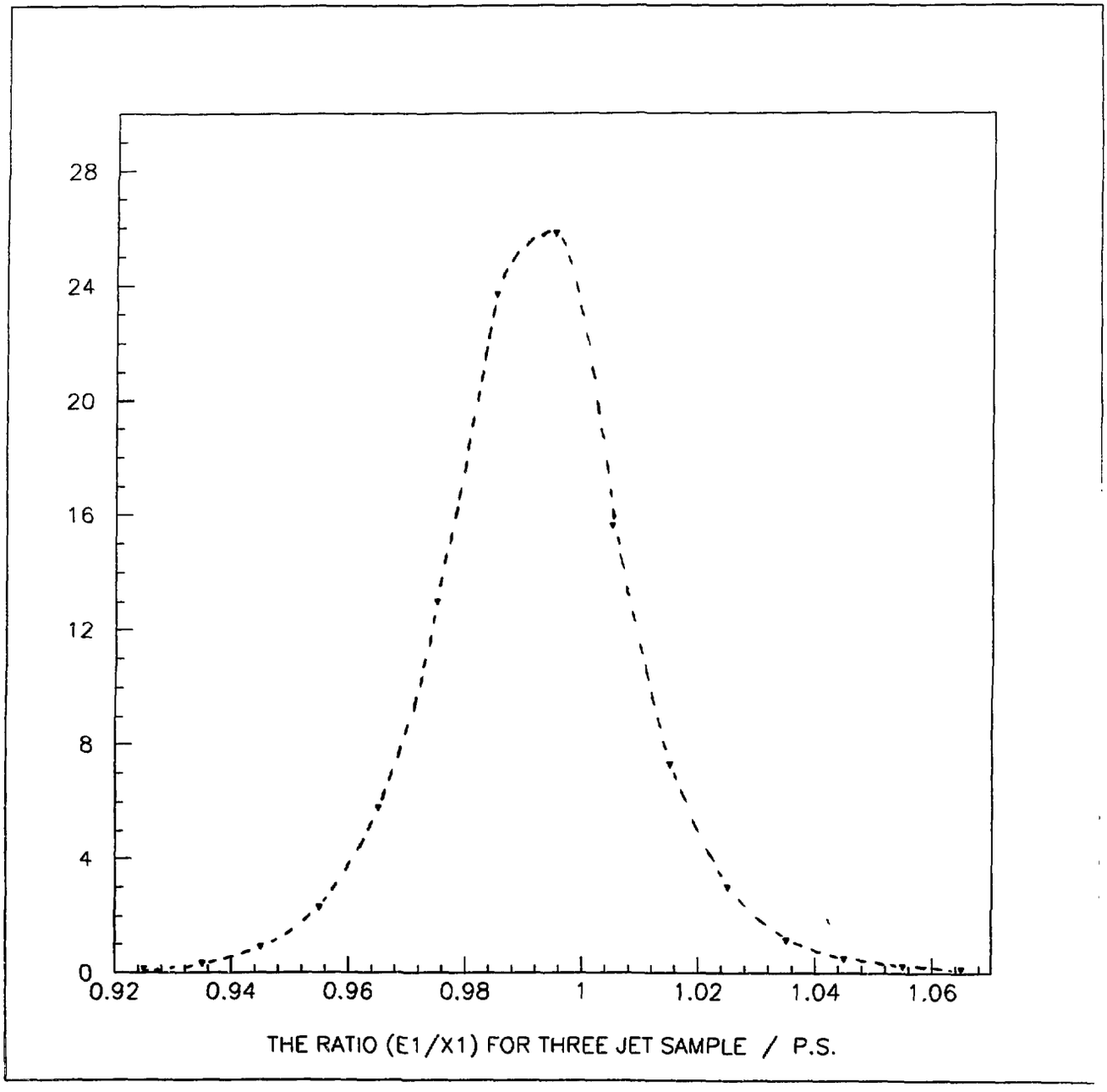
28
24
20
16
12
8
4
0
0.92
0.94
0.96
0.98
1
1.02
1.04
1.06
THE RATIO (E1/X1) FOR THREE JET SAMPLE / P.S.

Fig.3

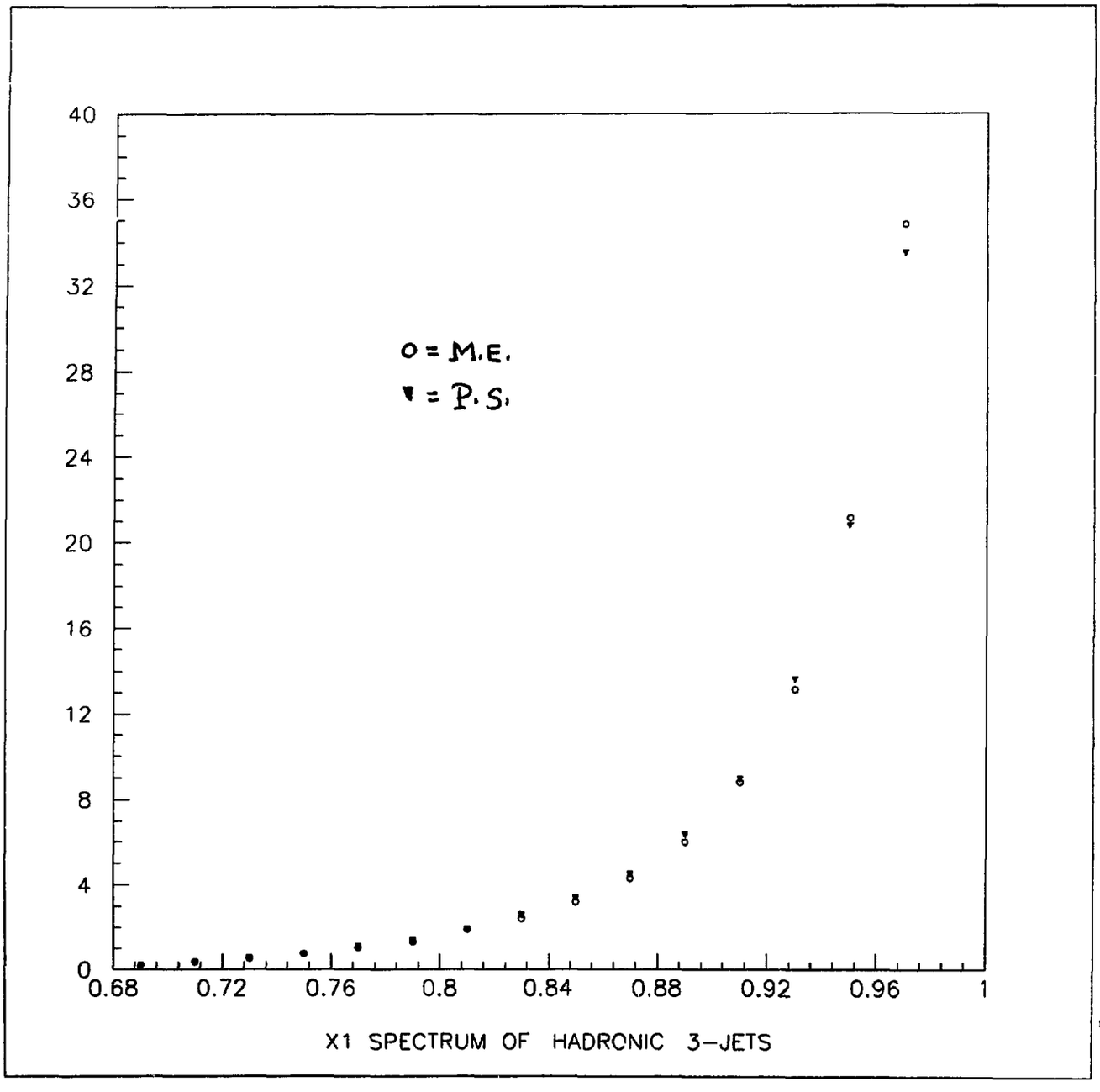
40
36
32
28
24
20
16
12
8
4
0
0.68
0.72
0.76
0.8
0.84
0.88
0.92
0.96
1
o = M.E.
▼ = P.S.
X1 SPECTRUM OF HADRONIC 3-JETS

Fig.4

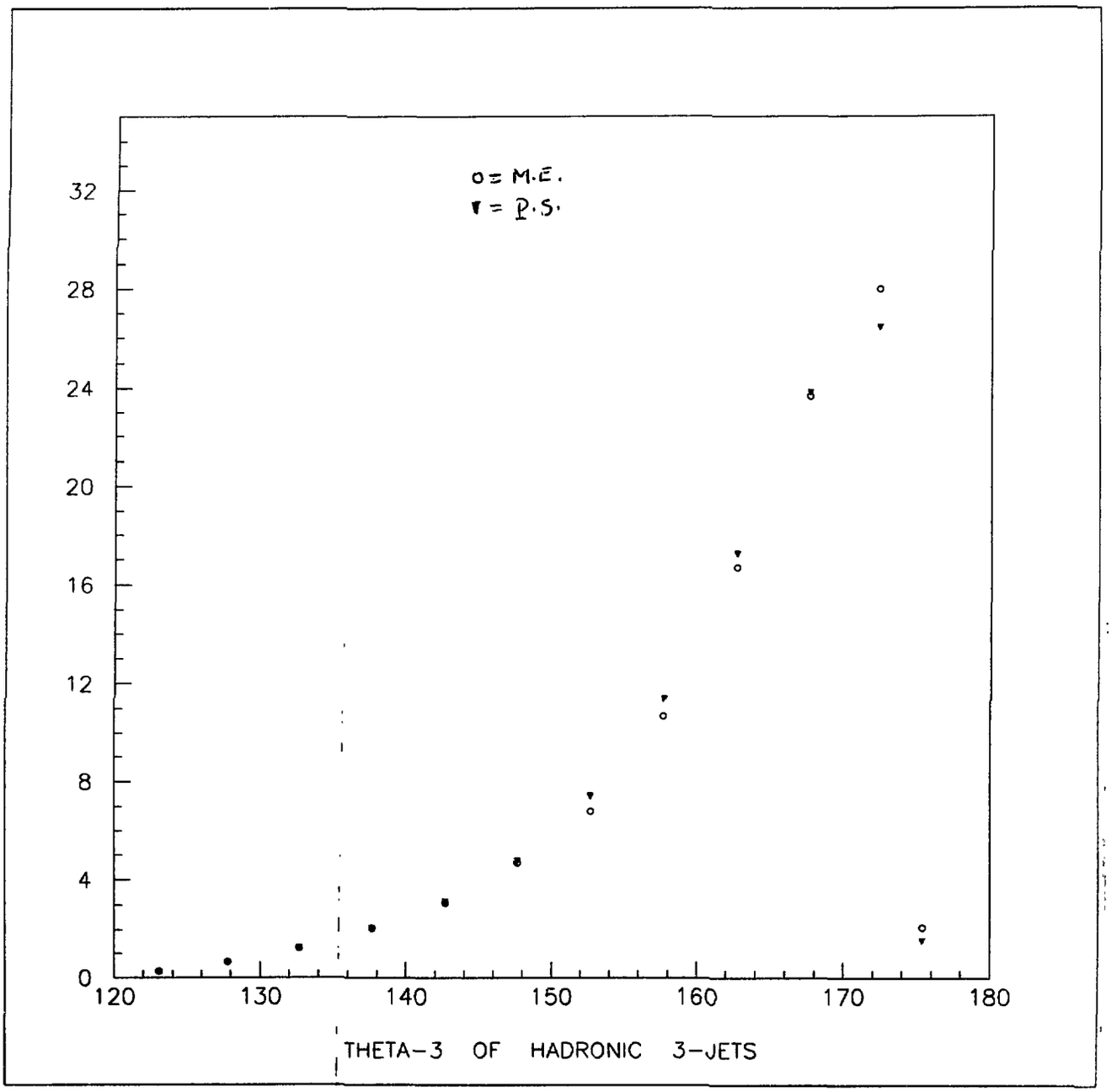
o = M.E.
▼ = P.S.
32
28
24
20
16
12
8
4
0
120
130
140
150
160
170
180
THETA-3 OF HADRONIC 3-JETS

Fig.5

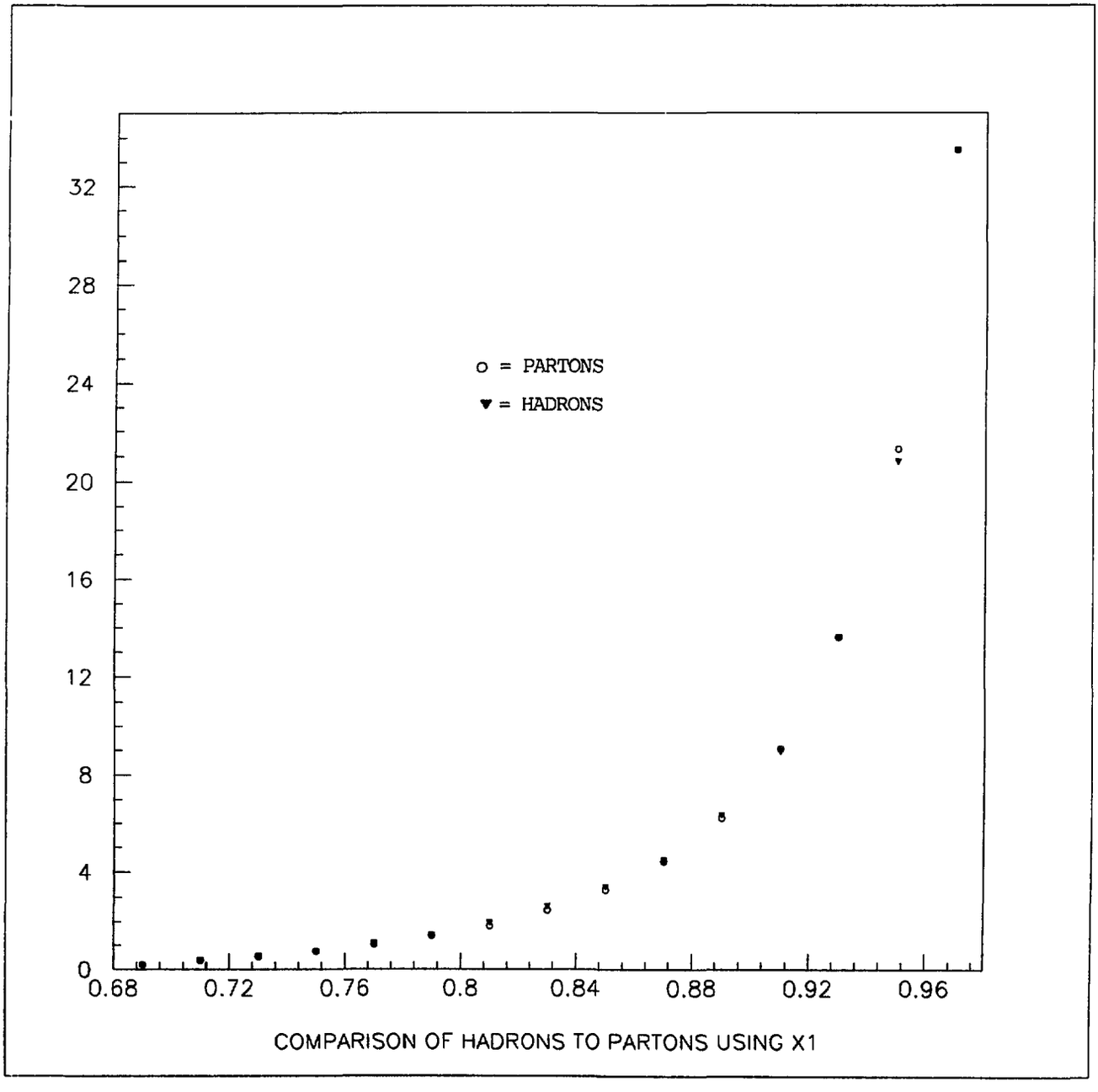

P.S. MODEL

Fig.6

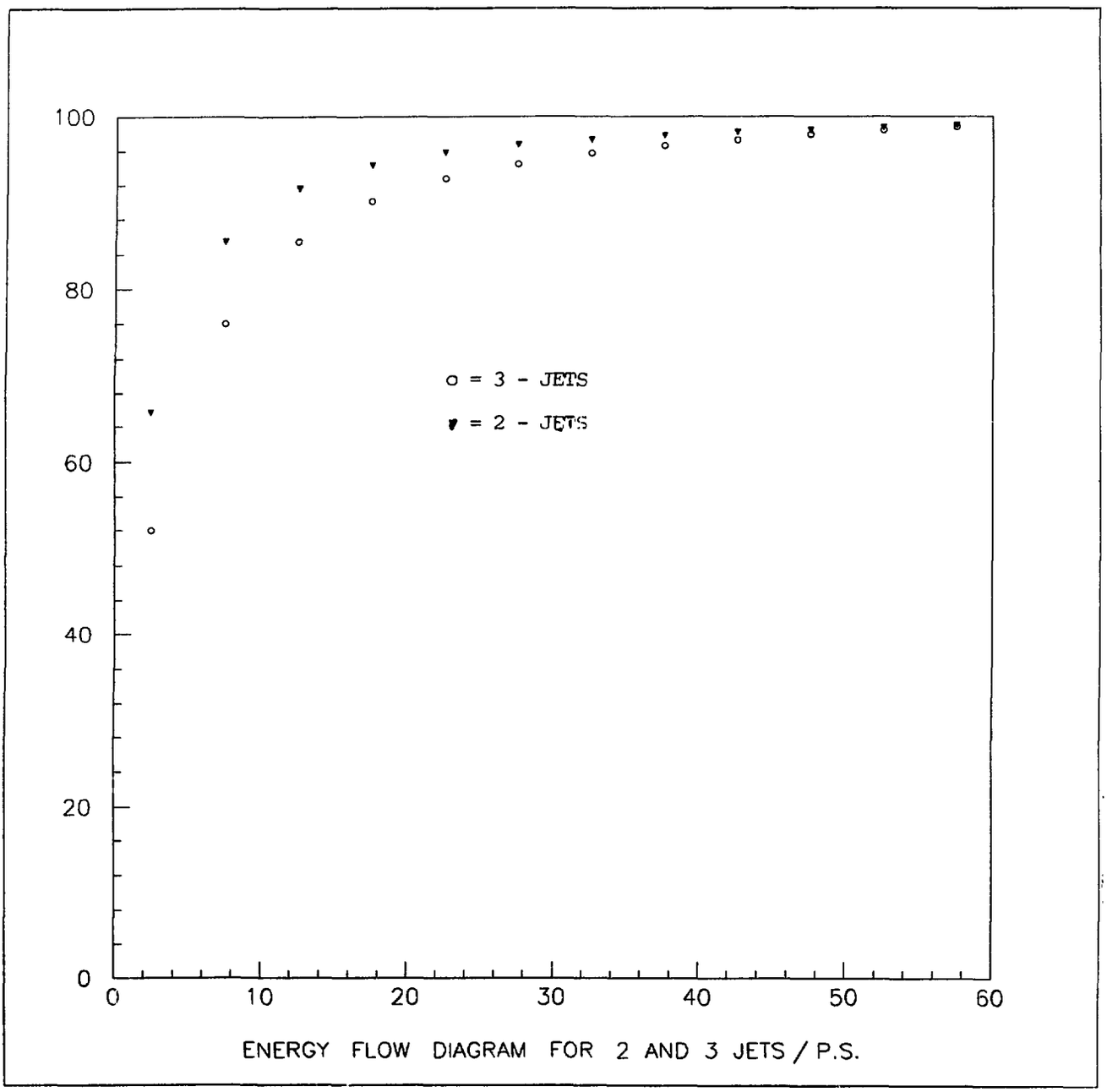
100
80
60
40
20
0
0
10
20
30
40
50
60
o = 3 - JETS
▼ = 2 - JETS
ENERGY FLOW DIAGRAM FOR 2 AND 3 JETS / P.S.

Fig.7

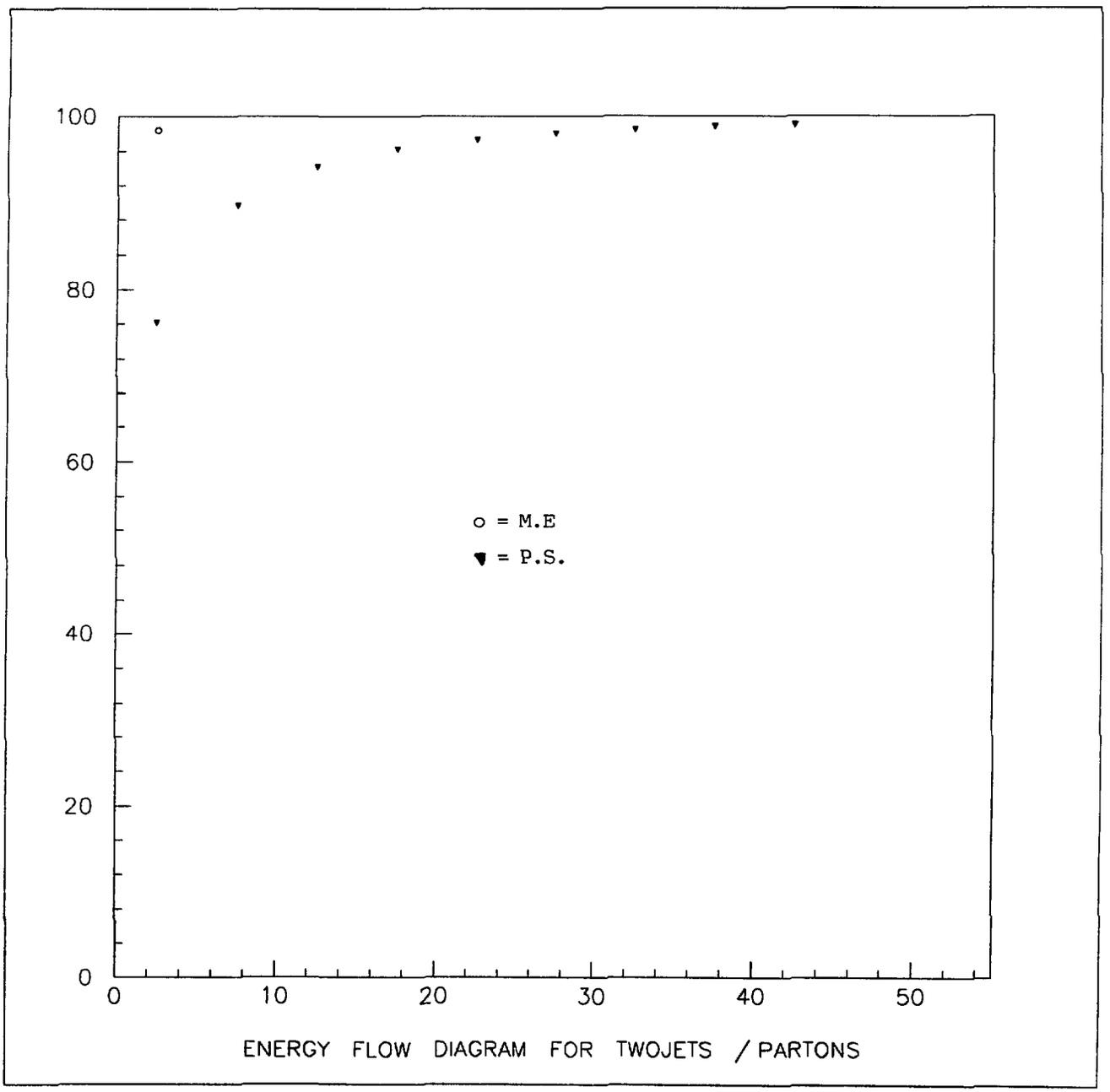
100
80
60
40
20
0
0
10
20
30
40
50
o = M.E
▼ = P.S.
ENERGY FLOW DIAGRAM FOR TWOJETS / PARTONS

Fig.8

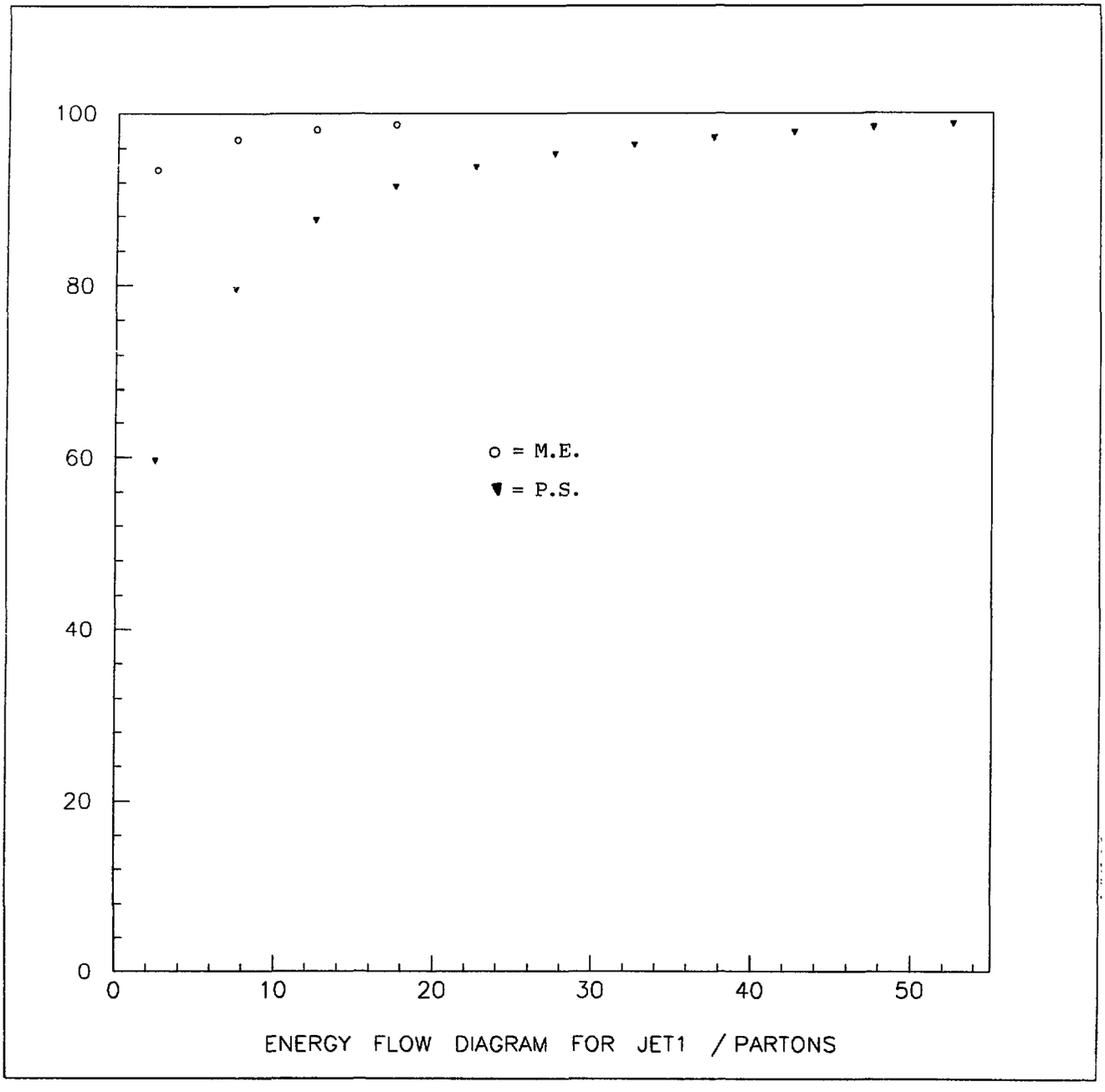
100
80
60
40
20
0
0
10
20
30
40
50
o = M.E.
▼ = P.S.
ENERGY FLOW DIAGRAM FOR JET1 / PARTONS

Fig.9

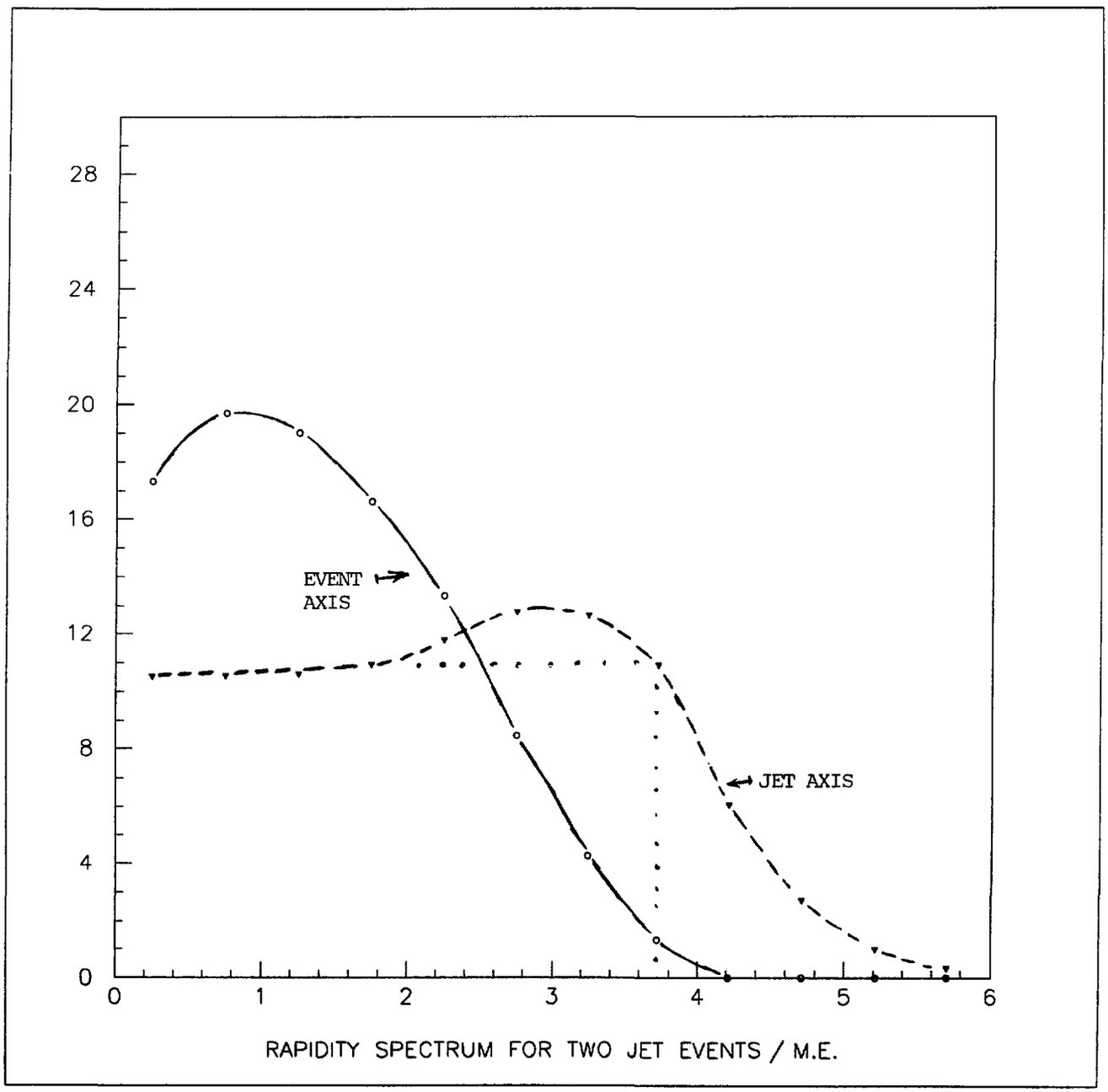
28
24
20
16
12
8
4
0
0
1
2
3
4
5
6
EVENT
AXIS
JET AXIS
RAPIDITY SPECTRUM FOR TWO JET EVENTS / M.E.

fig.10

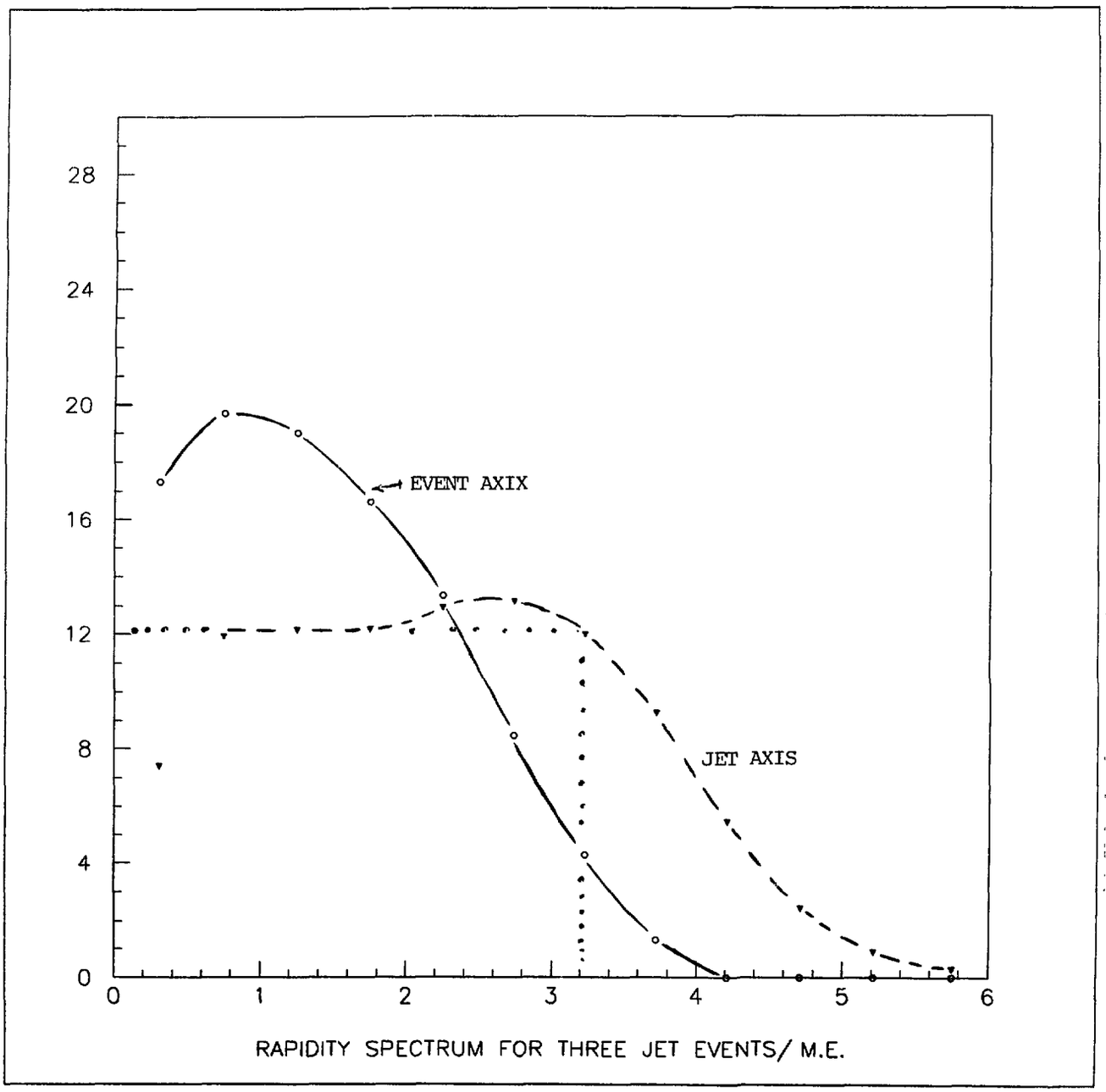
28
24
20
16
12
8
4
0
0
1
2
3
4
5
6
EVENT AXIX
JET AXIS
RAPIDITY SPECTRUM FOR THREE JET EVENTS/ M.E.

Fig.11

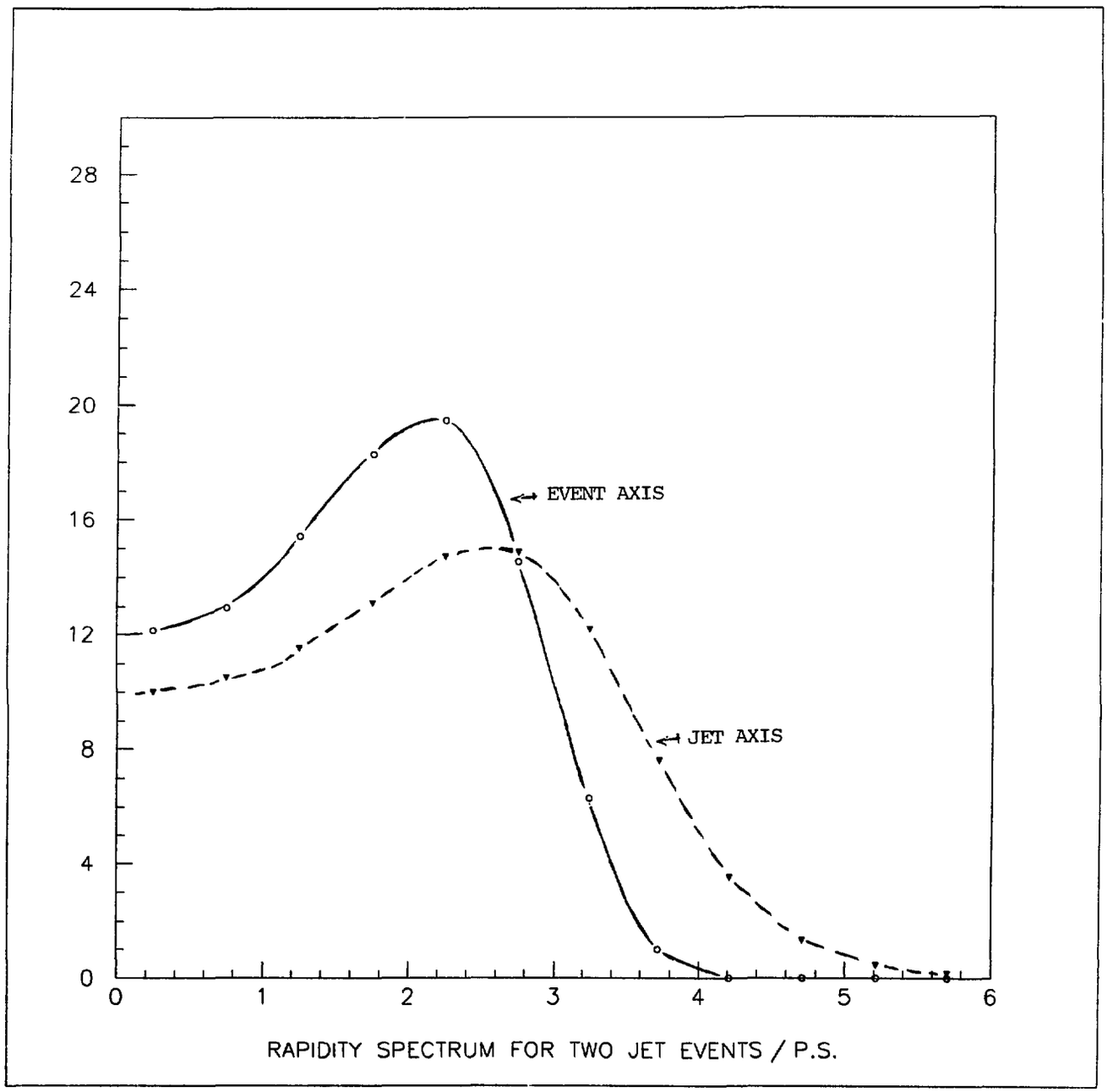
28
24
20
16
12
8
4
0
0
1
2
3
4
5
6
EVENT AXIS
JET AXIS
RAPIDITY SPECTRUM FOR TWO JET EVENTS / P.S.

Fig.12

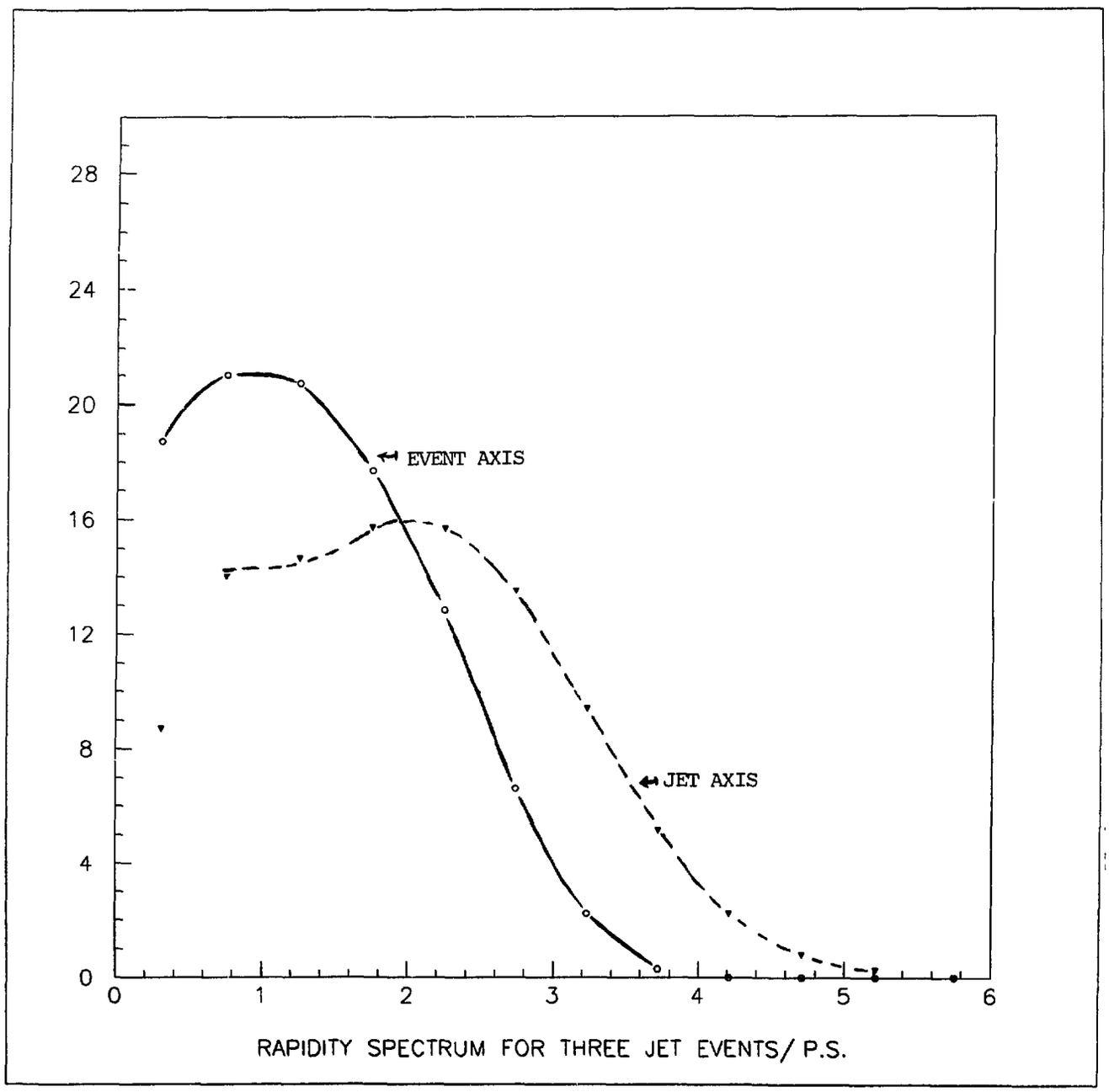
28
24
20
16
12
8
4
0
0
1
2
3
4
5
6
EVENT AXIS
JET AXIS
RAPIDITY SPECTRUM FOR THREE JET EVENTS/ P.S.

Fig.13

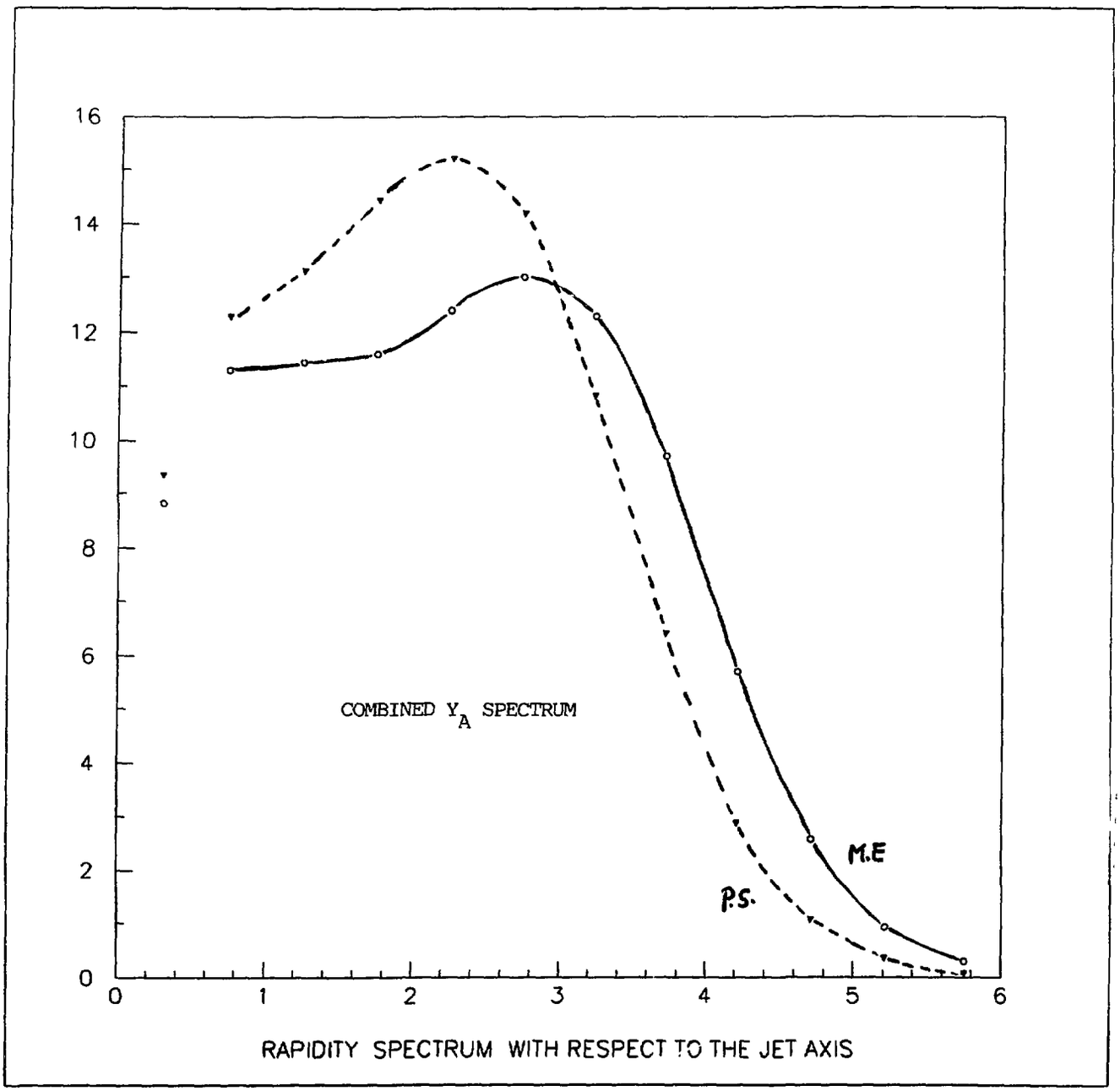
16
14
12
10
8
6
4
2
0
0
1
2
3
4
5
6
COMBINED Y_A SPECTRUM
M.E
P.S.
RAPIDITY SPECTRUM WITH RESPECT TO THE JET AXIS

Fig.14

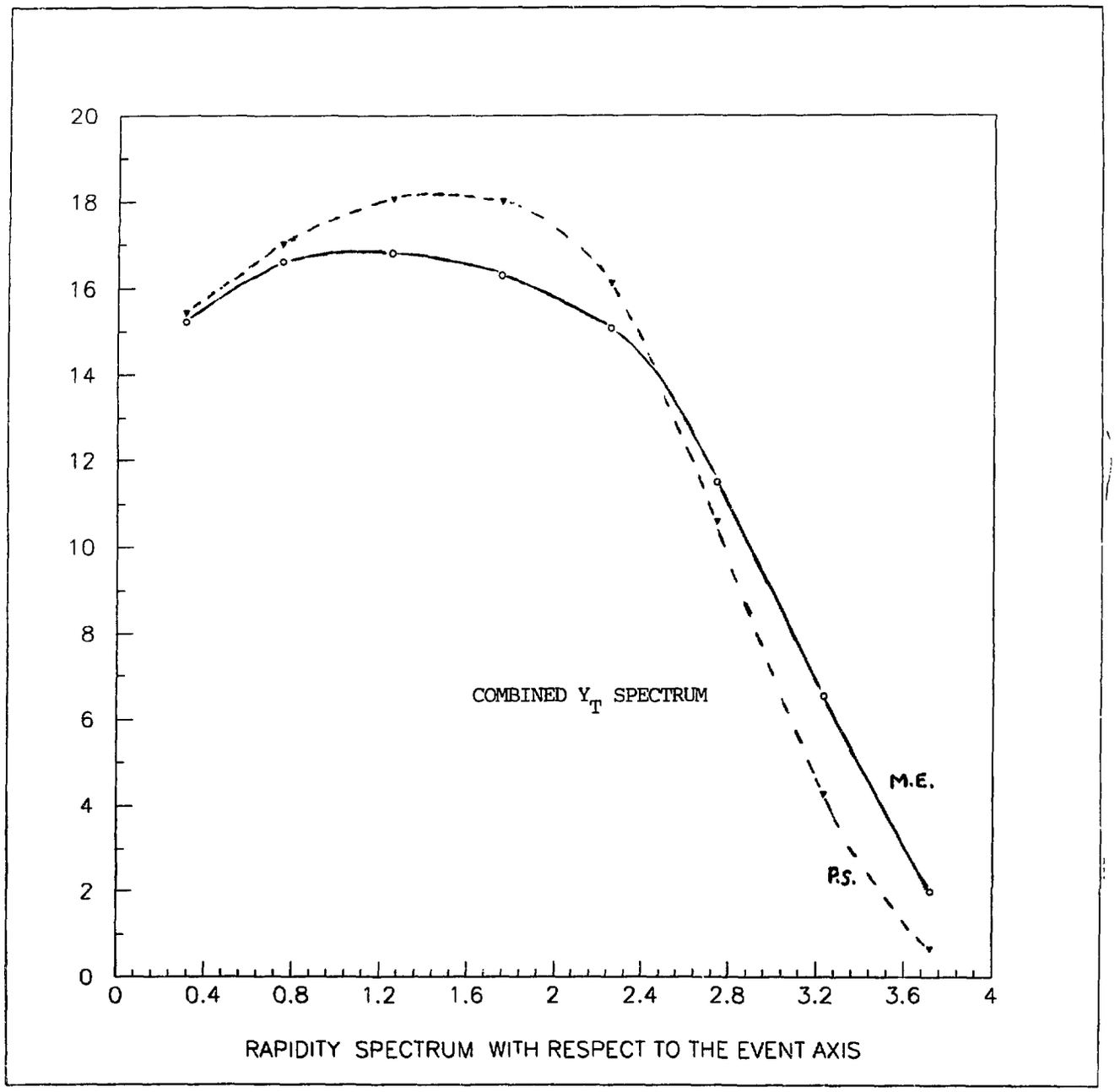
20
18
16
14
12
10
8
6
4
2
0
0
0.4
0.8
1.2
1.6
2
2.4
2.8
3.2
3.6
4
COMBINED Y_T SPECTRUM
M.E.
P.S.
RAPIDITY SPECTRUM WITH RESPECT TO THE EVENT AXIS

Fig.15

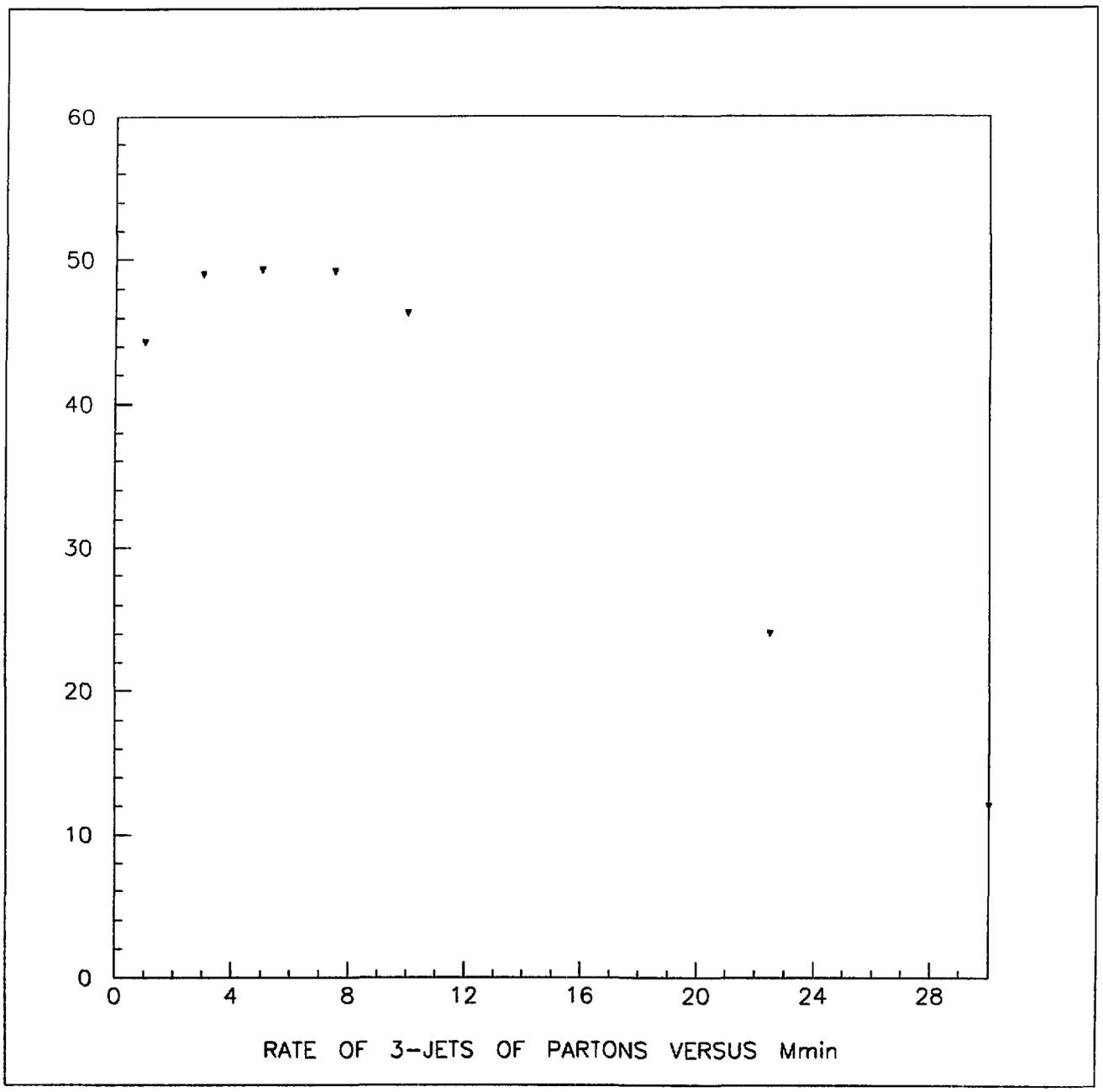
60
50
40
30
20
10
0
0
4
8
12
16
20
24
28
RATE OF 3-JETS OF PARTONS VERSUS Mmin

Fig.16

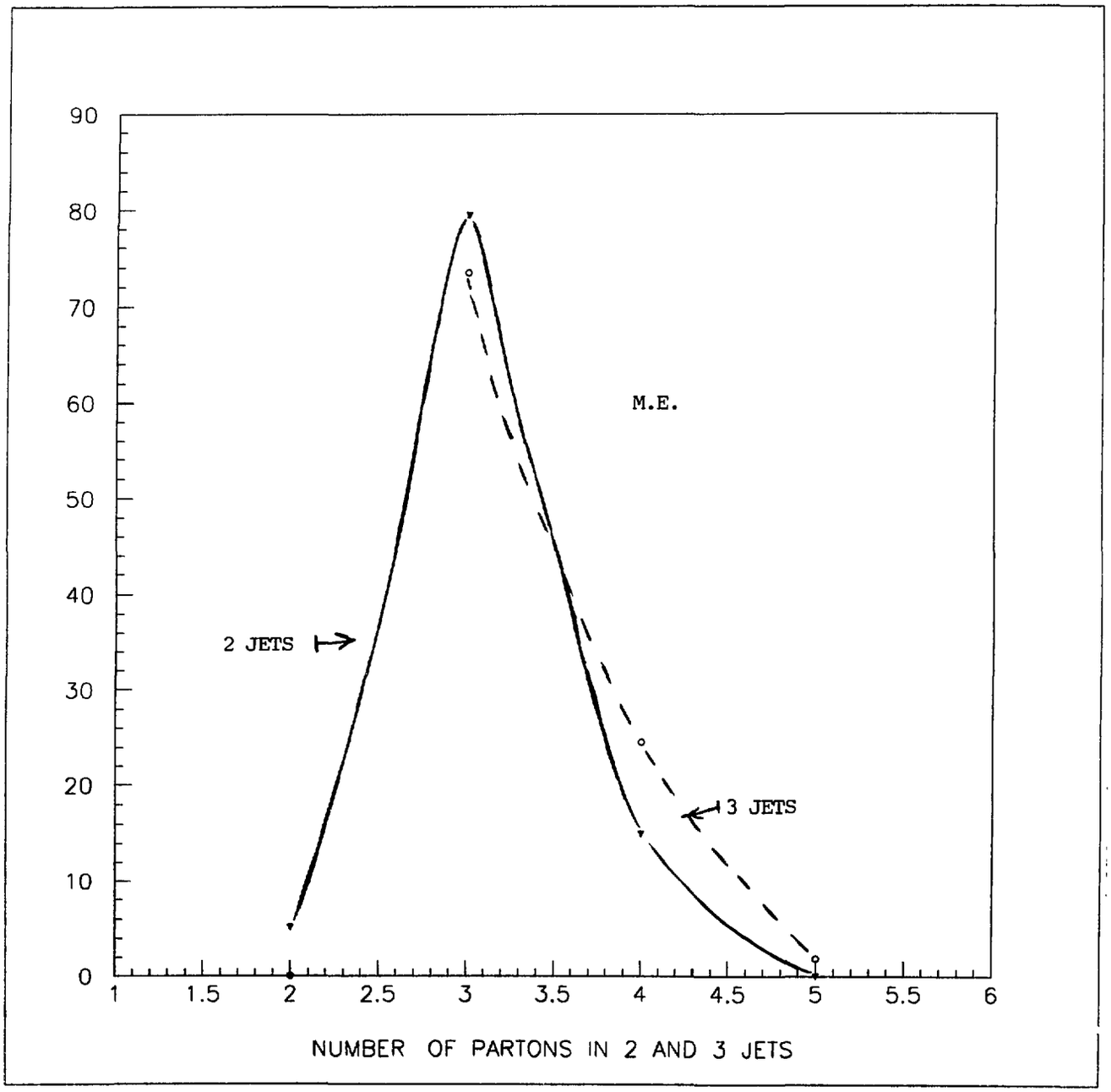
90
80
70
60
50
40
30
20
10
0
1
1.5
2
2.5
3
3.5
4
4.5
5
5.5
6
M.E.
2 JETS
3 JETS
NUMBER OF PARTONS IN 2 AND 3 JETS

Fig.17

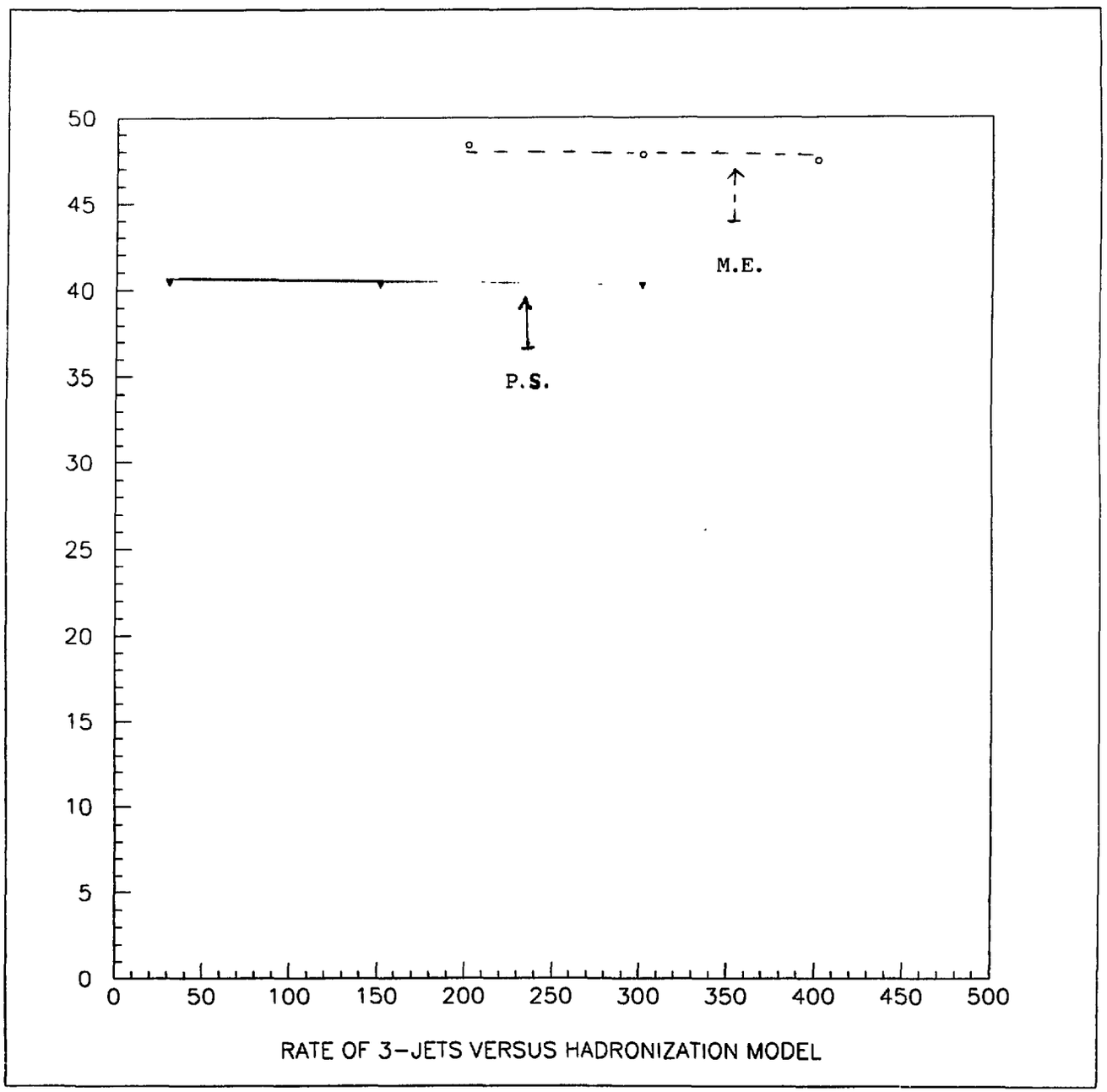
50
45
40
35
30
25
20
15
10
5
0
0
50
100
150
200
250
300
350
400
450
500
M.E.
P.S.
RATE OF 3-JETS VERSUS HADRONIZATION MODEL

Fig.18

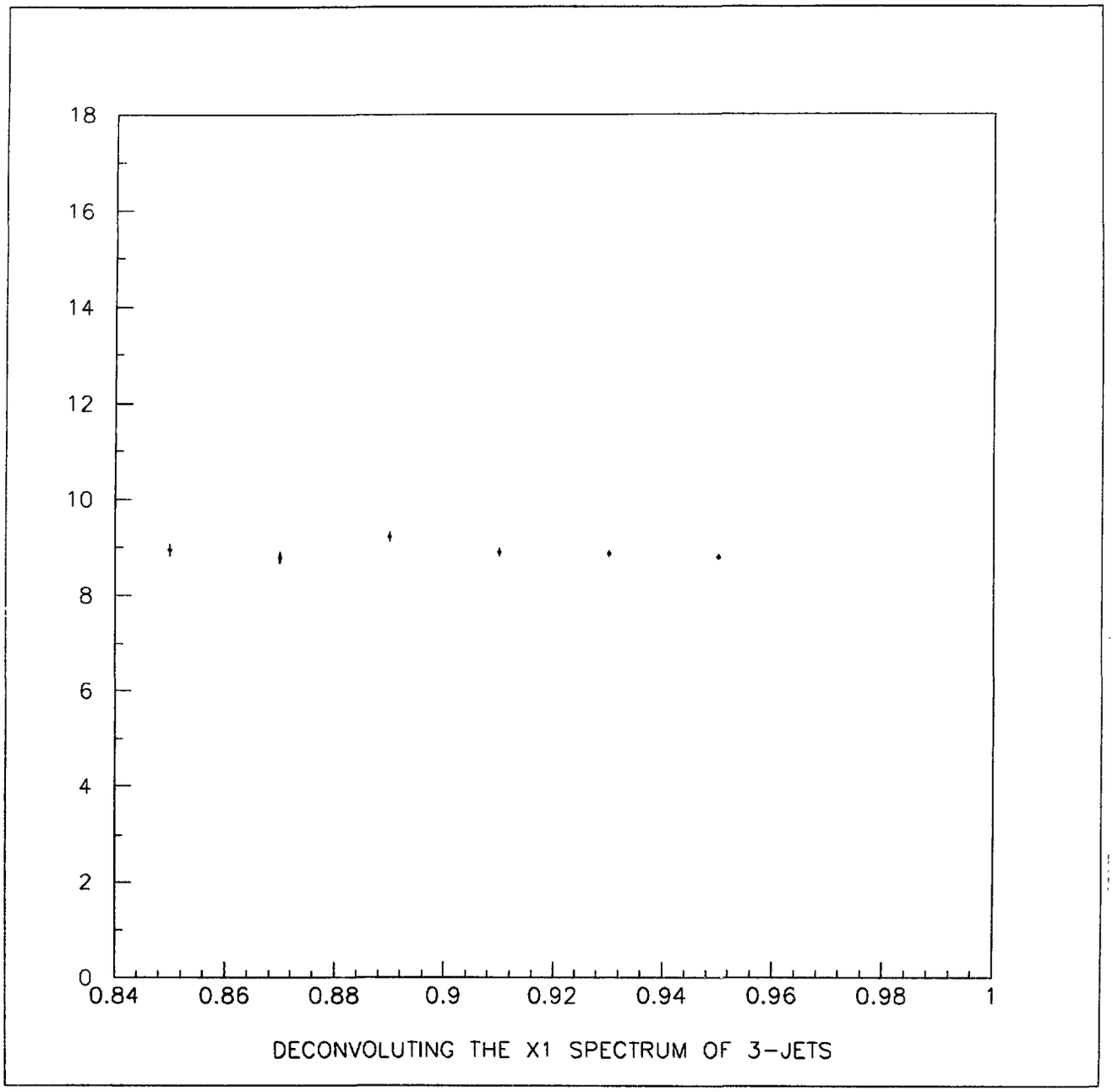
18
16
14
12
10
8
6
4
2
0
0.84
0.86
0.88
0.9
0.92
0.94
0.96
0.98
1
DECONVOLUTING THE X1 SPECTRUM OF 3-JETS

Fig. 19

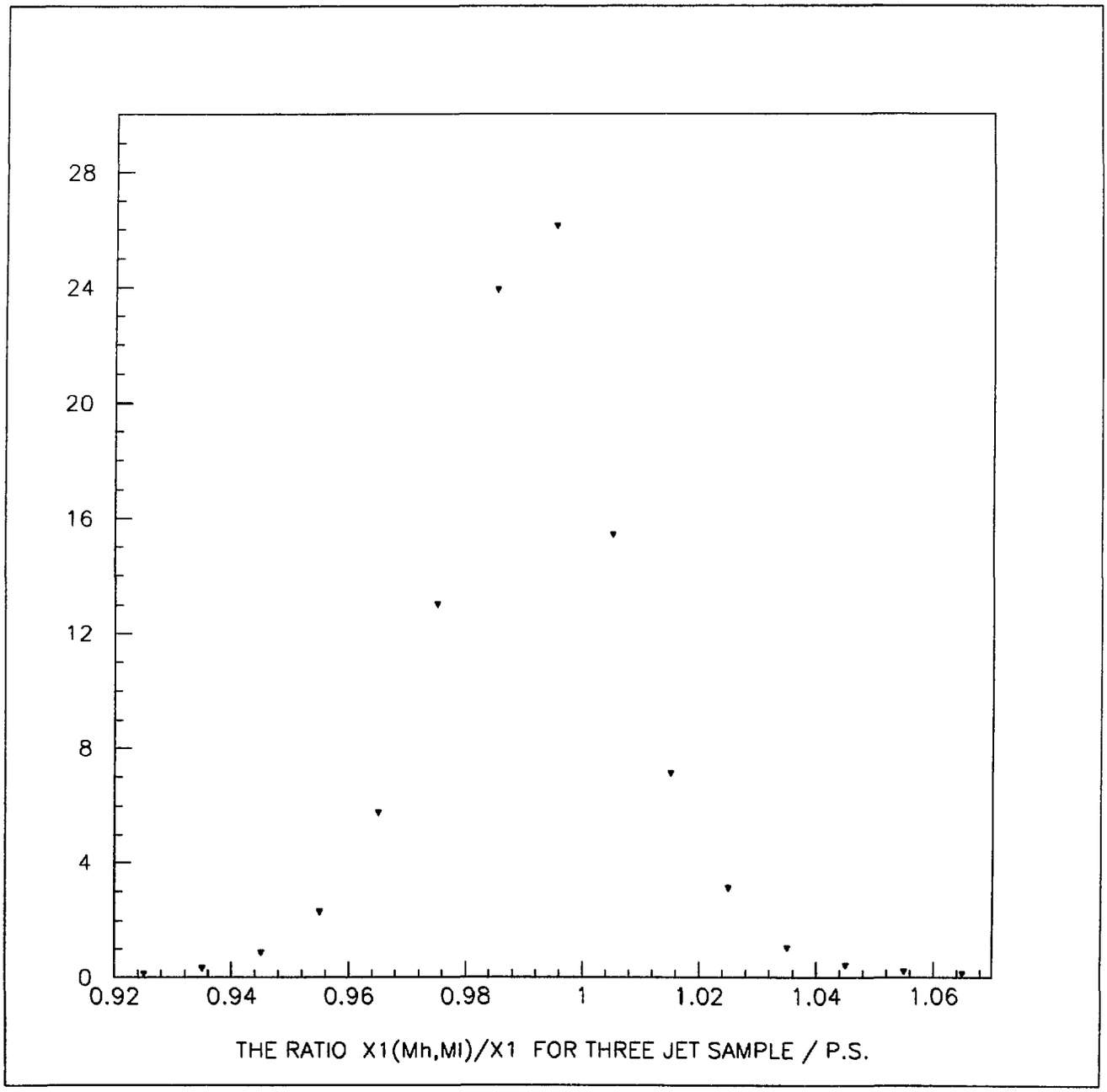
28
24
20
16
12
8
4
0
0.92
0.94
0.96
0.98
1
1.02
1.04
1.06
THE RATIO X1(Mh,MI)/X1 FOR THREE JET SAMPLE / P.S.

Fig.20

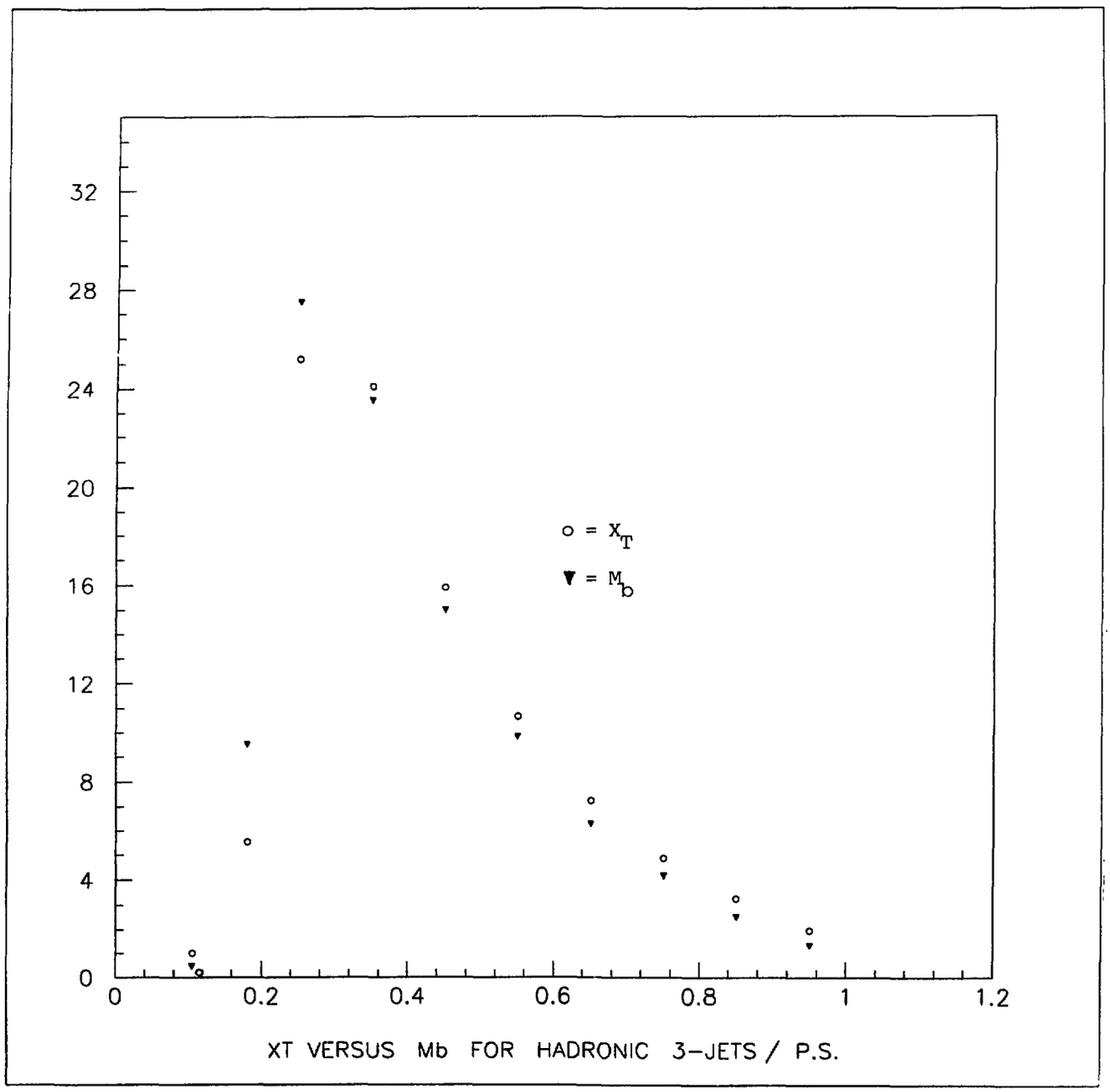
32
28
24
20
16
12
8
4
0
0
0.2
0.4
0.6
0.8
1
1.2
o = X_T
▼ = M_b
XT VERSUS Mb FOR HADRONIC 3-JETS / P.S.

Fig. 21

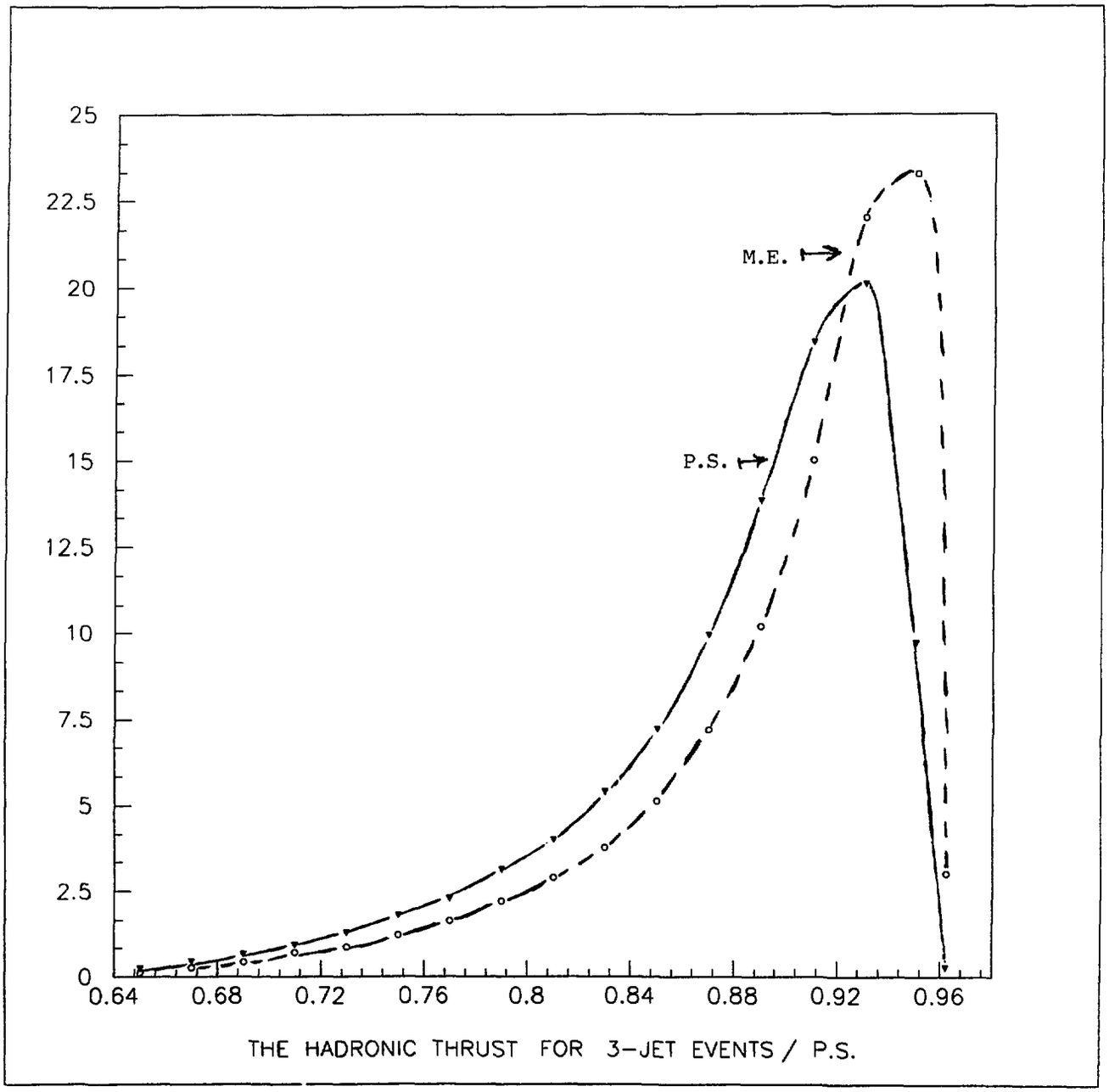
25
22.5
20
17.5
15
12.5
10
7.5
5
2.5
0
0.64
0.68
0.72
0.76
0.8
0.84
0.88
0.92
0.96
M.E.
P.S.
THE HADRONIC THRUST FOR 3-JET EVENTS / P.S.

Fig.22

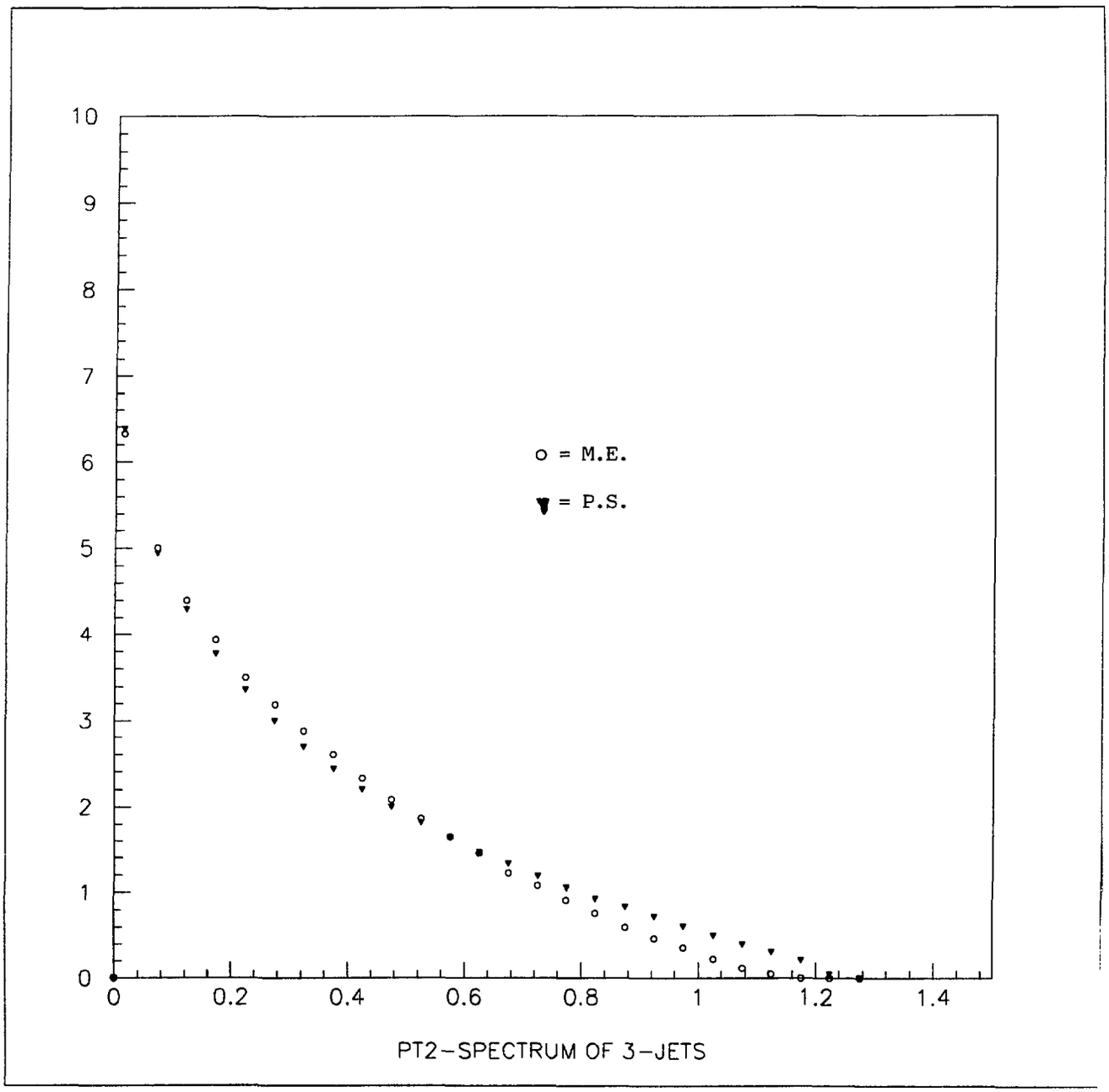

Fig.23

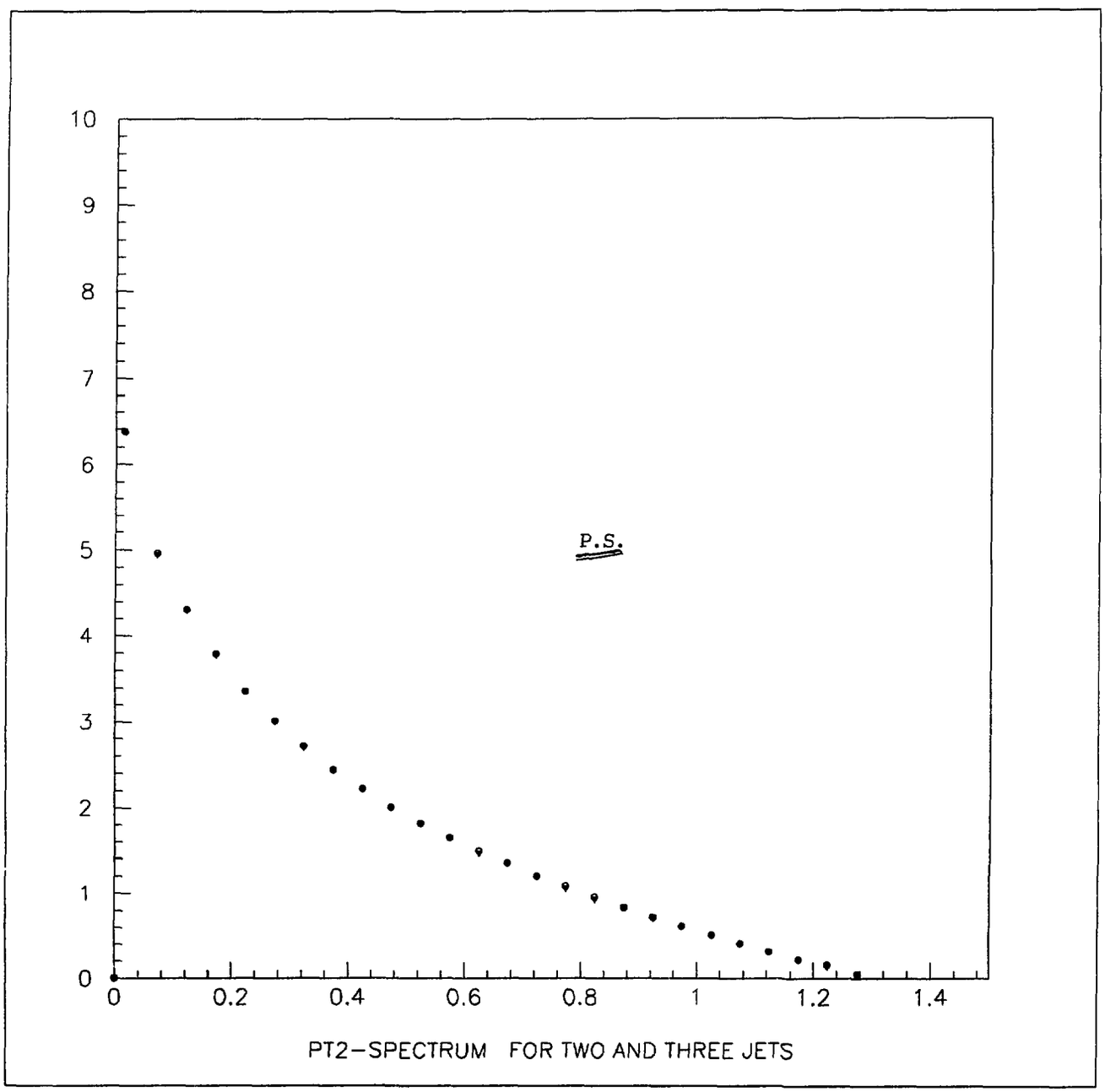
10
9
8
7
6
5
4
3
2
1
0
0
0.2
0.4
0.6
0.8
1
1.2
1.4
P.S.
PT2–SPECTRUM FOR TWO AND THREE JETS

Fig.24

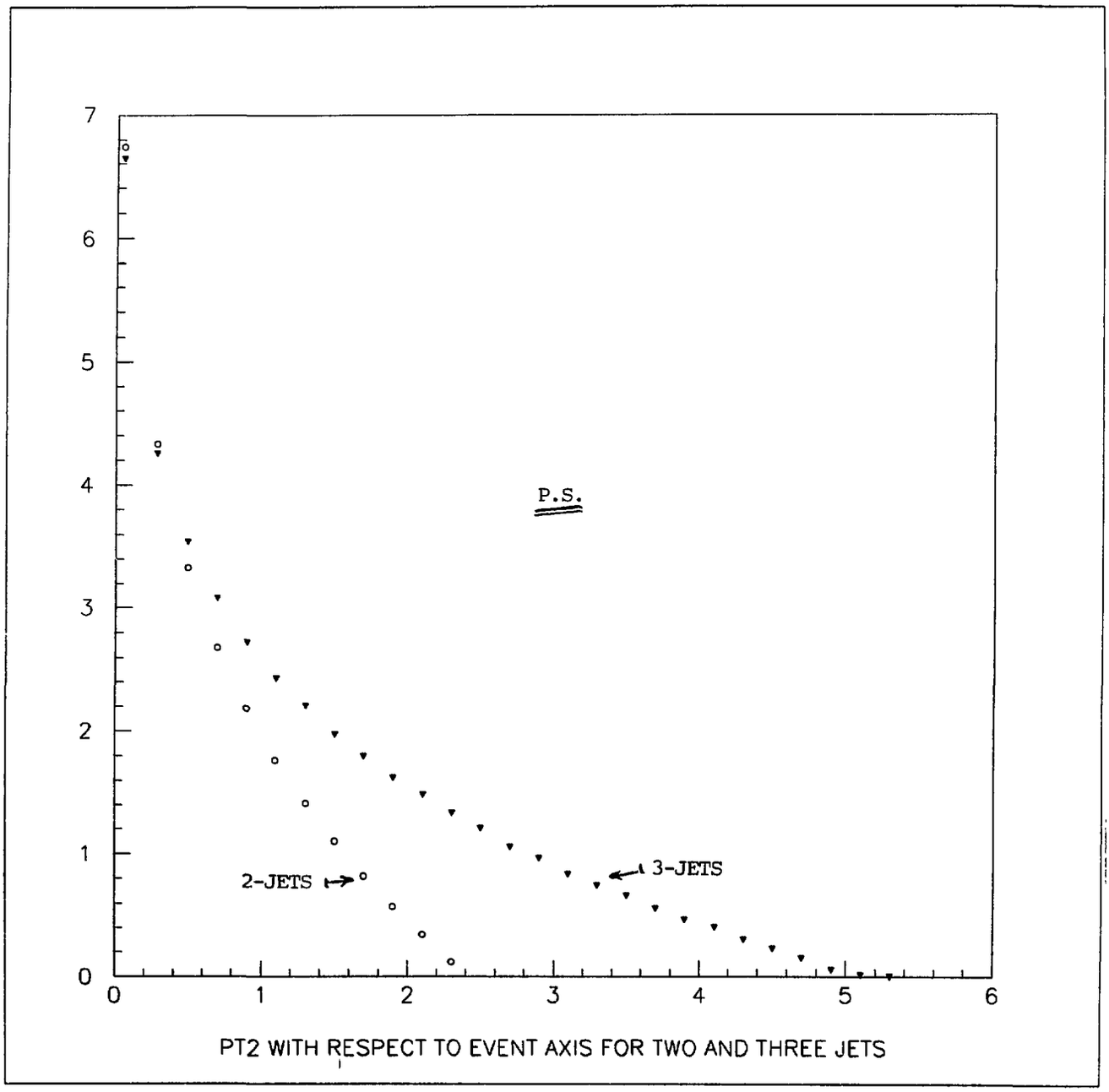
7
6
5
4
3
2
1
0
0
1
2
3
4
5
6
P.S.
2-JETS
3-JETS
PT2 WITH RESPECT TO EVENT AXIS FOR TWO AND THREE JETS

Fig.25

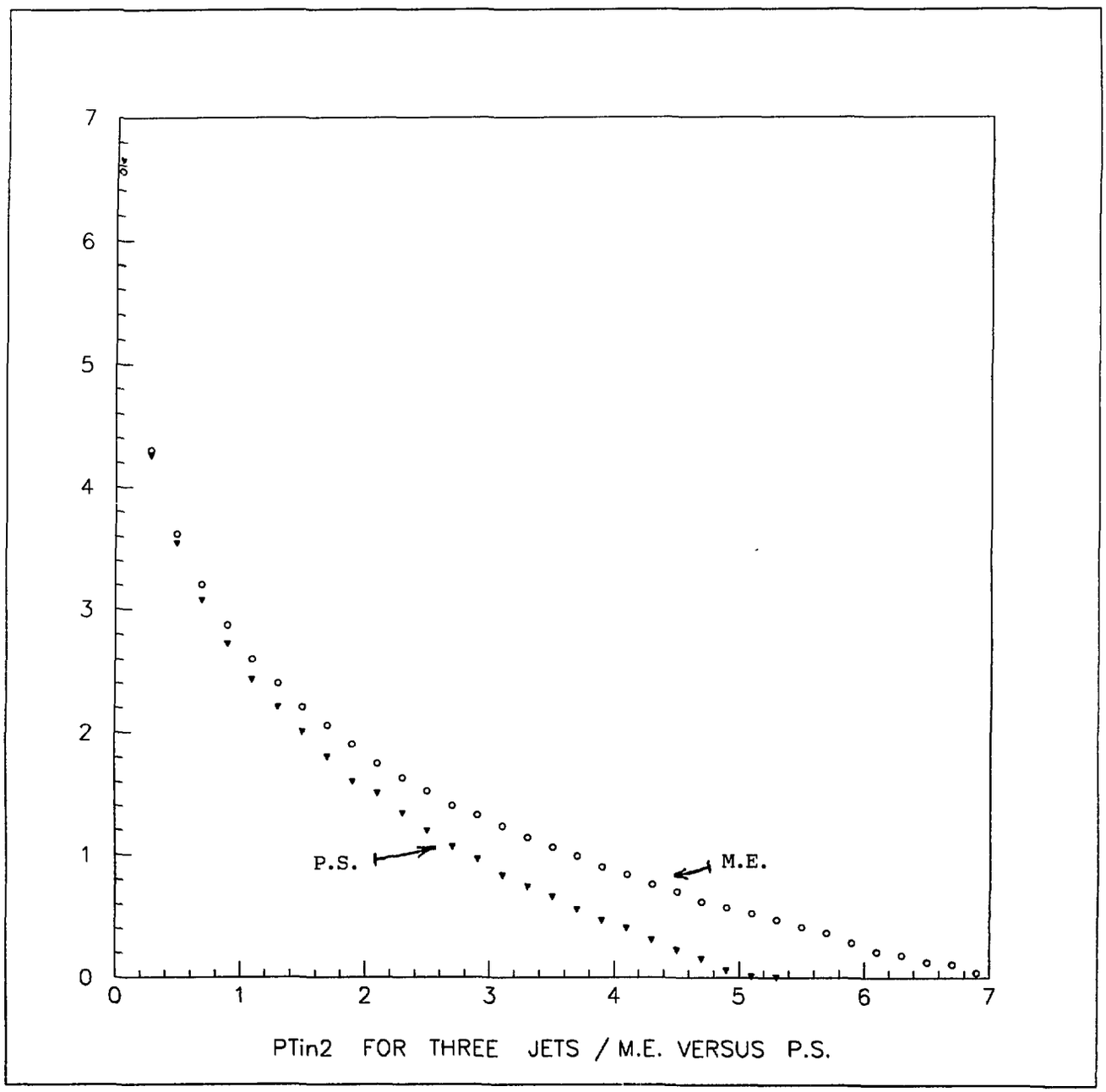

Fig.26